LAWRENCE
LIVERMORE
NATIONAL
LABORATORY

UCRL-TR-214984

Np and Pu Sorption to Manganese Oxide Minerals

P. Zhao, M. R. Johnson, S. K. Roberts, M. Zavarin

September 2, 2005

This work was performed under the auspices of the U.S. Department of Energy by University of California, Lawrence Livermore National Laboratory under Contract W-7405-Eng-48.

Np And Pu Sorption to Manganese Oxide Minerals

Pihong Zhao[1], Mackenzie R. Johnson[2], Sarah K. Roberts[2],
and Mavrik Zavarin[2]
[1]Chemical Biology and Nuclear Sciences Division
Chemistry and Materials Sciences Directorate
[2]Environmental Science Division
Energy and Environment Directorate
Lawrence Livermore National Laboratory
Livermore, California

Prepared for the Underground Test Area Project
U. S. Department of Energy
National Nuclear Security Administration
Nevada Site Office

Final Report
August 30, 2005

TABLE OF CONTENTS

LIST OF FIGURES

LIST OF TABLES

1 INTRODUCTION

Manganese oxide minerals are a significant component of the fracture lining mineralogy at Yucca Mountain (Carlos et al., 1993) and within the tuff-confining unit at Yucca Flat (Prothro, 1998), Pahute Mesa (Drellack et al., 1997), and other locations at the Nevada Test Site (NTS). Radionuclide sorption to manganese oxide minerals was not included in recent Lawrence Livermore National Laboratory (LLNL) hydrologic source term (HST) models which attempt to predict the migration behavior of radionuclides away from underground nuclear tests. However, experiments performed for the Yucca Mountain Program suggest that these minerals may control much of the retardation of certain radionuclides, particularly Np and Pu (Triay et al., 1991; Duff et al., 1999). As a result, recent HST model results may significantly overpredict radionuclide transport away from underground nuclear tests.

The sorption model used in HST calculations performed at LLNL includes sorption to iron oxide, calcite, zeolite, smectite, and mica minerals (Zavarin and Bruton 2004a; 2004b). For the majority of radiologic source term (RST) radionuclides, we believe that this accounts for the dominant sorption processes controlling transport. However, for the case of Np, sorption is rather weak to all but the iron and manganese oxides (Figure 1). Thus, we can expect to significantly reduce predicted Np transport by accounting for Np sorption to manganese oxides. Similarly, Pu has been shown to be predominantly associated with manganese oxides in Yucca Mountain fractured tuffs (Duff et al., 1999). Recent results on colloid-facilitated Pu transport (Kersting and Reimus, 2003) also suggest that manganese oxide coatings on fracture surfaces may compete with colloids for Pu, thus reducing the effects of colloid-facilitated Pu transport (Figure 1b). The available data suggest that it is important to incorporate Np and Pu sorption to manganese oxides in reactive transport models. However, few data are available for inclusion in our model. A survey of published data found only single-point (Triay et al., 1991; Kersting and Reimus, 2003; Keeney-Kennicutt and Morse, 1984; 1985) and qualitative (Duff et al., 1999; Dyer et al., 2000a; 2000b) Np and Pu sorption information.

This report describes recent experiments that quantified the sorption and desorption of Np(V) and Pu(IV) onto three manganese oxide minerals as a function of pH and time. The three manganese oxides (pyrolusite, birnessite, and hollandite[1]) have all been observed on fracture surfaces at Yucca Mountain and are likely to predominate at the NTS. Pyrolusite, birnessite, and hollandite comprise both a range of manganese oxide structure (framework, layered, and tunnel, respectively) and composition and a range of observed manganese oxide mineralogies. The pH range of 3-10 used in these experiments covers the range of pH observed in NTS groundwater (Rose et al., 1997).[2]

[1] Cryptomelane, the K^+ endmember of the hollandite group was used in our experiments.
[2] Of the 107 pH values reported by Rose et al. for southern Nevada groundwater (Table 2 in Rose et al., 1997), only one value was outside the experimental range: the water tested from one well in Area 12 of the NTS measured 10.5. Otherwise, the values listed all fell within pH 6.4-9.6.

Upon completion of sorption and desorption experiments, the sorption data were modeled based on surface complexation theory. The resulting reaction constants can be appended to the databases of Zavarin and Bruton (2004a; 2004b) for use in future HST modeling at the NTS. The sorption data are relevant to larger scale NTS radionuclide transport models as well.

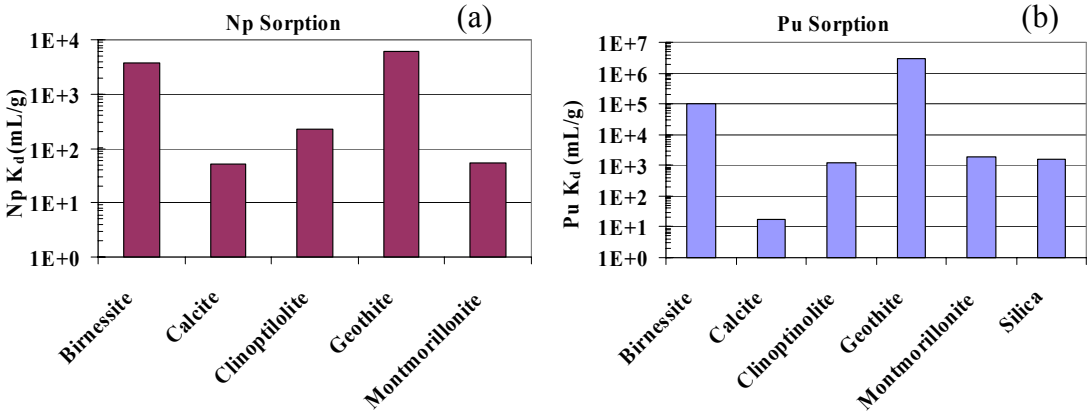

Figure 1. Np(V) sorption to various minerals at pH 8 and in J-13 surrogate waters (a) and Pu(V) sorption to various minerals at pH 8 and in J-13 surrogate waters (b). Note that Pu(V) is reduced to Pu(IV) on the mineral surfaces. Data from Kersting and Reimus (2003).

2 SORPTION DATA AVAILABLE IN THE LITERATURE

Manganese oxides (Mn oxides) form a large class of minerals often noted for their wide range of crystal structure, including minerals with tunnel and layer structures. General and detailed overviews of the various Mn oxide mineral compositions, structures, and occurrences can be found in Post (1999) and Waychunas (1991). X-ray absorption spectroscopy has further elucidated the crystal structure of several Mn oxides, and has been instrumental in advancing our understanding of the molecular interactions that occur during sorption (for instance: (Manceau *et al.*, 1992; Axe *et al.*, 2000; Trivedi *et al.*, 2001; Foster *et al.*, 2003; Shaughnessy *et al.*, 2003). Laboratory investigations of manganese oxide surface chemistry (Murray, 1974, 1975; Mckenzie, 1979; Balistrieri and Murray, 1982) have shown that they have a large surface area relative to other minerals and they have a high cation sorption capacity over a wide pH range (Tonkin et al., 2004). In the case of birnessite, the manganese oxide surface is negatively charged above pH ~2 which provides a strong negatively charged surface to which most positively charged cations readily sorb.

This class of minerals has been studied as a potential contaminant sorber for several decades, in part due to its ubiquitous presence in clays, soils and sediments (Tonkin et al., 2004). Most of the previous studies focused on the uptake of stable aqueous species by manganese oxides (Table 1). These studies can provide useful analog data for a number of radionuclides not examined in this report. While most of these radionuclides are not examined in this report, they comprise a significant fraction of the RST at the NTS. For instance, Al-Attar and Dyer (2002) investigated uranium sorption onto several ion-exchanged birnessites as a function of pH. They calculated different distribution coefficients for the different types of exchanged birnessites; maximum distribution coefficients (K_d) were measured at pH 6 (5.7×10^4 mL/ g for U sorption to Cs-exchanged birnessite) or at pH 4 (5.6×10^4 mL/g for U sorption to Co-exchanged birnessite). Misaelides et al. (2002) observed considerable sorption of Th, U and ^{233}Pa onto natural todorokite, a tunnel-structure manganese oxide, with maximum K_d values of 697, 94, and 6.3×10^4 mL/g, respectively.

With respect to Np and Pu, a number of published data are pertinent to the present study. Keeney-Kennicutt and Morse (Keeney-Kennicutt and Morse, 1984) found that $Np(V)O_2^+$ sorption to a synthetic MnO_2 and natural Mn nodule increased with decreasing ionic strength (most likely resulting from reduced competition between cations for surface sites). Compared to the Mn oxides, however, Np sorbed more strongly to iron oxide. Turin et al. (2002) observed a stronger correlation between Np sorption and iron oxide content than Np sorption and Mn oxide content. Interestingly, plutonium appears to exhibit the opposite behavior. Means et al. (1978) studied ^{244}Cm, ^{241}Am, and ^{238}Pu sorption onto soils near the Oak Ridge National Laboratory radioactive waste burial site. Duff et al. (1999), examined Pu(VI) sorption onto a natural zeolitic tuff. In both cases, researchers observed that Pu sorbed more strongly to Mn oxides than Fe oxides when both minerals were present.

Dyer et al. (2000a) reported that uptake of ^{236}Pu and other radionuclides by a synthetic birnessite was pH dependent. The Pu K_d at pH 9.1 was 39700 mL/g while at pH 1.2 and 13 it was 49 and 1620 mL/g, respectively. We would expect Np to exhibit pH dependent behavior as well.

Several researchers have attempted to model cation sorption to manganese oxides using a surface complexation approach. Catts and Langmuir (Catts and Langmuir, 1986) used a seven-variable model with monodentate complexation reactions to investigate uptake of several heavy metals onto δMnO_2. Smith and Jenne (Smith and Jenne, 1991) used those results in conjunction with the results from Balistrieri and Murray (1982) to constrain surface complexation constants in their triple layer model of metal adsorption onto iron and manganese oxides. Questioning the applicability of monodentate complexation reactions, Appelo and Postma (1999) formulated a new model to account for cation uptake by birnessite that incorporated diprotic sorption sites in a diffuse double layer model. More recently, Tonkin et al. (Tonkin *et al.*, 2004) developed a two-site diffuse double layer model using the data from seven earlier studies to develop a consistent set of surface acidity and divalent cation complexation constants. Nevertheless, just as there is a limited amount of experimental data available for radionuclide sorption onto Mn oxides, there are few publications that describe attempts to model the processes responsible for sorption.

Table 1. Manganese oxide sorption data available in the literature.

Element	Reference	Element	Reference
Ca	3, 11, 12, 19, 22, 27	Na	3, 11, 18, 26
Ni	6, 9, 19, 20, 27, 31	Mg	3, 19, 22, 27
Co	6, 11, 12, 16, 19, 25, 33	K	3, 18, 26
Sr	2, 6, 19, 22, 29, 30	Cr	13
Nb	28	Mn	6, 15, 19, 22
Cs	6, 26	Cu	4, 15, 27
Ce	10	Zn	4, 6,11, 12, 15, 19, 27, 30, 31
Sm	10, 28	As	7
Eu	10	Se	7, 13, 28
U	1, 13, 17, 28	Ag	22
Np	8, 28, 32	Ba	22
Pu	5, 6, 16, 23, 28, 32	Pb	4, 13, 14, 15, 21, 27
Am	16, 28, 32	Th	17, 28
Cm	16		

Key to references: 1) (Al-Attar and Dyer, 2002); 2) Axe et al., 2000; 3) Balistrieri and Murray, 1982; 4) Catts and Langmuir, 1986; 5) Duff et al., 1999; 6) Dyer et al., 2000a; 7) Foster et al., 2003; 8) Keeney-Kennicutt and Morse, 1984; 9) Kennedy et al., 2004; 10) Koeppenkastrop and Carlo, 1992; 11) Loganathan and Burau, 1973; 12) Loganathan et al., 1977; 13) Manceau et al., 1992; 14) Matocha et al., 2001; 15) Mckenzie, 1979; 16) Means et al., 1978; 17) Misaelides et al., 2002; 18 and 19) Murray, 1974, 1975; 20) Olin and Lehikoinen, 1997; 21) O'Reilly and Hochella, 2003; 22) Posselt et al., 1968; 23) Shaughnessy et al., 2003; 24) Stahl and James, 1991; 25) Tamura et al., 1997; 26) Tanaka and Tsuji, 1997; 27) Tessier et al., 1996; 28) Triay et al., 1997; 29 and 30) Trivedi and Axe, 1999, 2001; 31) Trivedi et al., 2001; 32) (Turin et al., 2002); and 33) Zachara et al., 1995.

3 SORPTION EXPERIMENT METHODS

3.1 Manganese Oxide Preparation

Pyrolusite, birnessite, and cryptomelane were chosen for sorption-desorption experiments based on their common occurrence at Yucca Mountain (Carlos et al., 1993). Mineralogic analysis of Mn-oxides at the NTS has not been performed, though the presence of Mn-oxides is well known. It is expected that the Mn-oxide mineralogy at NTS will be similar to that observed at Yucca Mountain. Natural samples of these Mn oxide minerals rarely occur in pure form and could not be purchased. As a result, synthetic minerals were used. While synthetic pyrolusite could be purchased, birnessite and cryptomelane were synthesized using recipes from the literature.

3.1.1 Pyrolusite

Reagent grade MnO_2 was purchased from Mallinckrodt Baker, Inc. chemical supplies. XRD analysis confirmed that this black powder was crystalline, chemically pure pyrolusite (Figure 2). Powder x-ray diffraction (XRD) patterns of each mineral were collected on a Scintag Pad V diffractometer with Cu-K_α radiation.

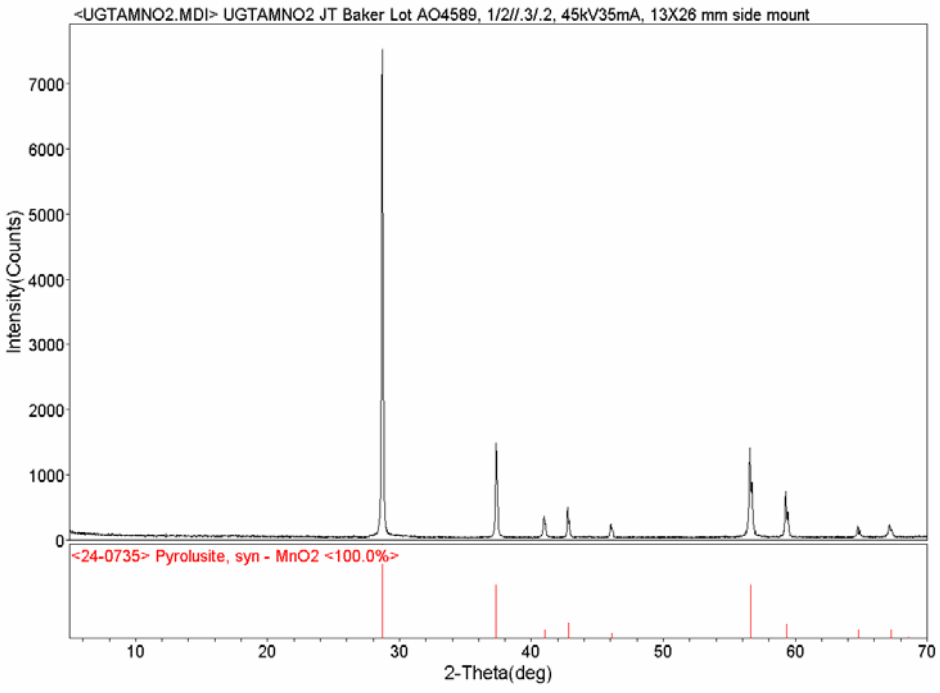

Figure 2. XRD pattern of purchased pyrolusite.

3.1.2 Birnessite and Cryptomelane

Birnessite was synthesized according to the methods outlined by (Golden *et al.*, 1986). After adding 250 mL of 5.5M NaOH to 200 mL of 0.5M $MnCl_2$, oxygen was bubbled into the resulting $Mn(OH)_2$ suspension, usually through a glass frit, at a minimum rate[3] of 3.6 ft^3 hr^{-1} (1.7 L min^{-1}) for 5 hours. When the recipe was doubled or quadrupled, the oxygen was introduced into the suspension for 6 or 8 hours, respectively.
After oxygenation, the suspension was divided into 250 mL HDPE bottles and 50 mL polycarbonate centrifuge tubes and the precipitates were separated from the solution using an International Equipment Company Centra-8 centrifuge (5 minutes at 2200 RPM). The supernatant was discarded and the precipitates were rinsed 8-10 times with Milli-Q purified water and then freeze dried for at least 24 hours with a LABCORP Freeze Dryer 4.5 lyophilizer. The resultant black powder was examined using XRD analysis and the identified peaks (Figure 3) confirmed the presence of crystalline birnessite ($Na_{0.55}Mn_2O_4 \bullet 1.5\ H_2O$). A single run yielded approximately 8-9 g of product.

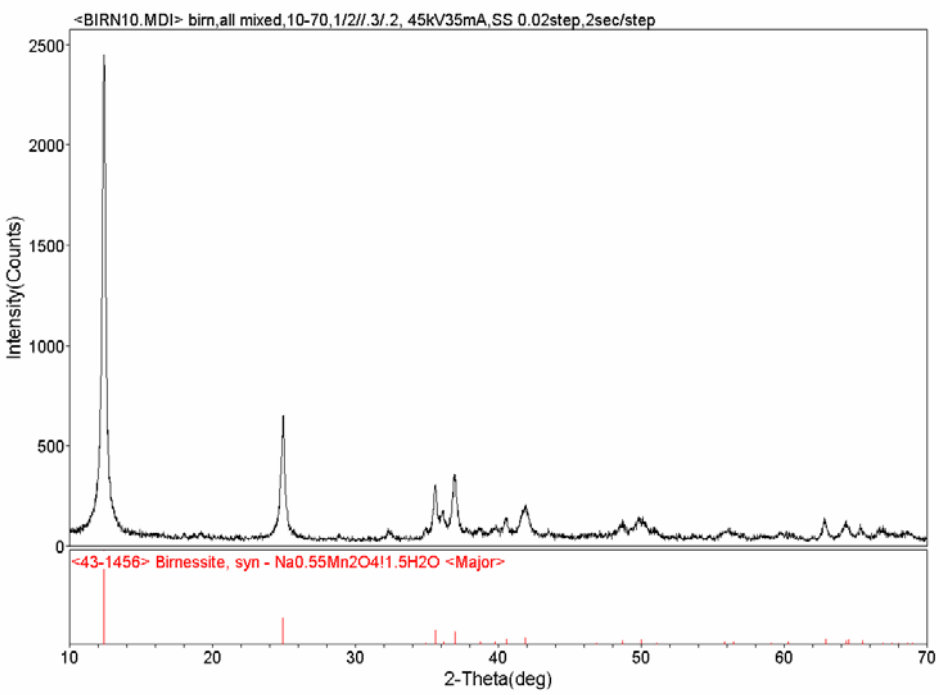

Figure 3. XRD pattern of synthetic birnessite.

To synthesize cryptomelane, the recipe of Chen et al. (Chen *et al.*, 1986) was used. Portions of synthetic birnessite were washed and centrifuged 8 times with 1M KCl to initiate ion exchange between the Na in the birnessite and the K in solution. The

[3] During one synthesis, the oxygen regulator was incorrectly adjusted such that the flow was much lower than the 3.6 ft^3 hr^{-1} minimum that the meter displayed. It became obvious after this run that the minimum flow rate is crucial because the resultant mineral was hausmannite (Mn_3O_4).

precipitates were then rinsed 5 times with Milli-Q water to remove any excess KCl. Five rinses resulted in supernatant conductivity values of 75 to 130 µS. The rinsed precipitates were then placed in an oven at 200˚C. The temperature was raised by 200˚C every two hours until a final temperature of 800˚C was achieved. After the minerals had been at 800˚C for 2 hours they were placed in a 25˚C oven to cool overnight before being examined by XRD. The XRD pattern (Figure 4) indicated that the resultant black powder was a mixture of vernadite ($Mn(OH)_4$) and cryptomelane ($K_2Mn_8O_{16}$) with some sodium impurities resulting from incomplete Na-K exchange between the birnessite and the KCl solution.

During Pu(IV) sorption experiments using these two minerals, it was observed that the solution pH increased dramatically. It suggested that excess hydroxide remained in the dried solids. As a result, prior to starting Np(V) sorption experiments, the birnessite and cryptomelane were rinsed several times in weak $NaNO_3$ and KNO_3 solutions, respectively. The rinses affected the measured surface area of the birnessite, but did not significantly alter the surface area of the cryptomelane (see Section 4.2).

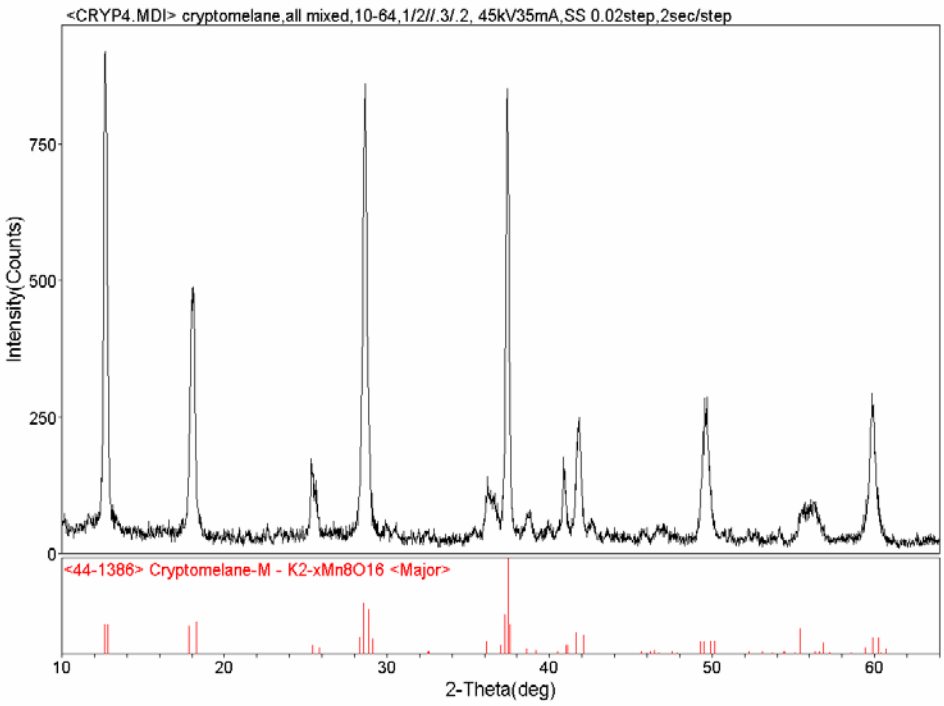

Figure 4. XRD pattern of synthetic cryptomelane.

3.2 Sorption and Desorption Experiments

3.2.1 Np(V)

A stock solution of Np(V) (8.10×10^{-4} mol L^{-1}) in 1M HNO_3 was used as the spike solution in the sorption experiments. The oxidation state of Np(V) was confirmed using a Guided Wave Model 260 Fiber Optic spectrophotometer. A Tri-Carb 2500 Liquid Scintillation analyzer from Packard Instrument Company was used for liquid scintillation counting (LSC) of the α-emitter ^{237}Np. An α,β discrimination mode was used in LSC for ^{237}Np to reduce the counting interference from β-emitter ^{234}Pa, a daughter of ^{237}Np. Gamma spectrometry with a high purity germanium detector was used for accurate nuclear counting at 29.4 keV to determine the concentrations of ^{237}Np in the stock and reference solutions.

A small spike (≤ 20 μL) of the Np(V) stock was added to each of 8 reaction tubes filled with 50 mg of each manganese oxide mineral and 35mL of a synthetic groundwater ranging in pH from 3 to 10. The synthetic groundwater solutions were based on a 4.5 x 10^{-3} mol L^{-1} $NaHCO_3$ solution with pH adjusted using HNO_3 or NaOH. The synthetic groundwater had been allowed to pre-equilibrate at room temperature (23 ± 2˚C) for up to a week with the 50 mg of manganese oxide mineral prior to starting the sorption experiment. The pH of each reaction tube was re-adjusted using NaOH and/ or HNO_3 if a large deviation from initial pH was observed during the pre-equilibration period. A Np(V) spike was added only after the pH in the reaction tubes stabilized. Np(V) was added to achieve an initial concentrations of $3.4\text{x}10^{-6}$ mol L^{-1} Np(V). All the reaction tubes were continuously rotated end-over-end to ensure thorough mixing during the experiment. At the prescribed sampling intervals, solutions were centrifuged for 5-10 minutes @ 5000 RPM prior to sampling the supernatant. A negligible volume of supernatant was sampled at 1 day, 15 days and ~30 days and analyzed for ^{237}Np using LSC. The pH of each sorption solution was not adjusted, only monitored during each sampling. After the 30 day sampling, the remaining supernatant was sampled and analyzed for carbonate alkalinity, cation, and anion concentrations.

The partition coefficient (K_d, mL/g) obtained from sorption and desorption experiments was calculated using equations (1) and (2), respectively.

$$K_d = \frac{(A_i - A)}{A} \times \frac{V}{m} \quad (1)$$

$$K_d = \frac{\%Sorption}{100 - \%Sorption} \times \frac{V}{m} \quad (2)$$

where A_i and A are the activity (cpm mL^{-1}) of Np or Pu in the supernatant before and after it contacted the manganese oxides, respectively; m is the mass (g) of the minerals used; and V is the volume (mL^3) of solution. The %*Sorption* was calculated in desorption

experiments from the total activity of Np or Pu in each sample and the activity in the aqueous phase.

At the end of the 30 day sorption experiment, the solids containing sorbed Np were mixed with 35 mL radionuclide-free solution to start the desorption experiments (pHs were kept the same). All the reaction tubes were continuously rotated during the desorption experiment (~33 days). The supernatants were sampled at 1 day, 15 days and ~30 days. At the end of the 30 day desorption experiment, the oxidation state of Np was characterized using solvent extraction.

3.2.2 Pu(IV)

The Pu(IV) stock solution (2.96×10^{-7} mol L^{-1}) used in the sorption experiments was purified from ^{241}Am, the β-decay daughter of ^{241}Pu, using a TEVA resin (Eichrom Technologies, Inc.) column, then the final effluent was diluted into 1 M HNO_3. The total Pu contained in the stock solution was comprised of 7.03% ^{238}Pu, 87.2% ^{239}Pu, 5.57% ^{240}Pu, 0.153% ^{241}Pu and 0.051% ^{242}Pu by mass, as determined by α-spectrometry. Due to the low Pu concentration of the Pu stock solution, the Pu oxidation state could not be confirmed using the standard UV/VIS spectrometric technique; instead we used a solvent extraction method with 4-Benzoyl-3-methyl-1-phenyl-2-pyrozolln-5-one (PMBP)[4]. The extraction results showed that >90±5% of Pu was Pu(IV). A Tri-Carb 2500 Liquid Scintillation analyzer from Packard Instrument Company was used for Pu α-LSC.

A spike (≤ 20 μL) of the Pu(IV) stock was added to each of 8 reaction tubes filled with 35 mL of pH 3 to 10 sodium bicarbonate solutions. The background solutions had been allowed to pre-equilibrate for up to 3 days at room temperature (23 ± 2˚C) with 10 mg of each manganese oxide mineral. The pH of each solution was re-adjusted using NaOH and/ or HNO_3 if a large deviation from initial pH was observed during the pre-equilibration period. After the pH in the reaction tubes stabilized, the tubes were spiked with Pu(IV) to achieve an initial Pu(IV) concentration of 5×10^{-9} mol L^{-1}. All the reaction tubes were continuously rotated to ensure thorough mixing during the reaction time (~34 days). The supernatant, separated from the Pu-sorbed minerals by centrifugation for 5-10 minutes at 5000 RPM, was sampled after 1 day, 15 days and ~34 days, and analyzed for Pu using α–LSC. The pH of each sorption solution was not adjusted, only monitored during each sampling. At the end of the sorption experiment, the supernatant was analyzed for carbonate alkalinity, cation, and anion concentrations.

For the desorption experiment, the solid phases, containing sorbed Pu, were mixed with 35 mL of pH-adjusted radionuclide-free solution. All the reaction tubes were constantly rotated during the reaction time (~23 days). The supernatants were sampled after 1 day, 15 days and 23 days. At the end of desorption experiments, the oxidation state of Pu in the supernatant and on the minerals was characterized using solvent extraction.

[4] See Section 4.4.3 on page 36.

3.3 Oxidation State Analysis

Organic chemical reagents 4-benzoyl-3-methyl-1-phenyl-2-pyrozolln-5-one (PMBP) and bis(2-ethylhexyl) hydrogen phosphate (D2EHPA) contain functional groups that can chelate the +4 and +4/+6 Np (or Pu) oxidation states, respectively. In our experiments, these two chemical reagents, dissolved in xylene, were used to extract Np and Pu species into the organic phase from a 1 N HCl solution and quantify the fractions of +4 and +6 oxidation states. Sodium dichromate quantitatively oxidizes +3 to +4 and +5 to +6 species in 1 N HCl. When combined with PMBP and D2EHPA extractions, we can quantify the fraction of +3, +4, +5, and +6 Np (or Pu) oxidation states in solution. We used the combination of dichromate oxidation and organic extraction to determine the percentage of each Np and Pu oxidation state in desorption solutions and on the mineral surfaces.

The procedure for determining oxidation state was as follows:

Mix 0.8-4 mL of Pu/Np containing aqueous solution with 0.2-1 mL 5 N HCl and 0.5-1 mL PMBP/xylene or D2EHPA/xylene solvent in a centrifuge tube; shake the tube vigorously for > 5 minutes on a Vortex shaker/mixer. Finally, centrifuge the tube for 1 minute at >3000 RPM to separate the aqueous and organic phases. The aqueous phase is extracted twice by each organic chelating reagent, and a sample of 0.4 to 1 mL from each phase is taken for α-LSC. The PMBP extraction yields +4 species. The D2EHPA extraction yield +4 and +6 species.

Next, 0.8-4 mL of Pu/Np containing aqueous solution is reacted with 0.2-1 mL of a 0.02 mol L^{-1} $Na_2Cr_2O_7$ solution. This reaction oxidizes all +3 species to +4 and all +5 species to +6. The oxidized solution is then extracted with either PMBP or D2EHPA as described above. The PMBP extraction yields +3 and +4 species. The D2EHPA extraction yields +4, +5, and +6 species. The results from all four extractions are used to calculate the fractions of +3, +4, +5, and +6 species.

3.4 Modeling Approach

The modeling approach was based on a mechanistic description of the aqueous speciation and surface complexation of radionuclides. We refer the reader to recent summary documents that describe the surface complexation modeling approach and relevant aqueous speciation constants (Zavarin and Bruton 2004a; 2004b). In those documents, the authors describe a database of non-electrostatic surface complexation and ion exchange reactions that model the sorption of several radionuclides (including Np and Pu) to iron oxide, calcite, and aluminosilicate minerals. The results described in this report provide the needed information to expand our modeling approach and include additional sorption reaction relevant to accurately predict radionuclide sorption at the NTS: surface complexation to manganese oxide minerals.

Aqueous speciation and surface complexation modeling was accomplished using the Geochemist's Workbench (Bethke, 2002) or the FITEQL program (Herbelin and Westall,

1999). A surface complexation model for birnessite was developed by Tonkin et al. (2004) and is used as the foundation for our modeling of Np(V) sorption data. Some modeling using the earlier model of Appelo and Postma (1999) is also discussed. Models of cation sorption to cryptomelane and pyrolusite have not been reported in the literature. As a result, no attempt was made to model sorption to those minerals. However, we discuss the relationship between the birnessite, cryptomelane, and pyrolusite data; in general, we found that the behavior of all three minerals is similar. Pu sorption data were not modeled because it was found that the Pu oxidation state changed during the experiments; furthermore, oxidation state changes appeared to be pH dependent. Due to this complex behavior, Pu sorption modeling was not attempted.

4 RESULTS AND DISCUSSION

4.1 Aqueous Speciation of Pu and Np(V) and Surface Speciation of Birnessite

The redox chemistry of Np is simple relative to Pu. In NTS-type, low ionic strength sodium bicarbonate groundwaters, Np predominantly occurs in the +5 oxidation state as the NpO_2^+ ion (Keeney-Kennicutt and Morse, 1984) and forms carbonate or hydroxide species depending on the pH and carbonate alkalinity of the solution. While changes in the redox state of Np(V) were not expected, the Np oxidation state was examined at the end of desorption experiments (see Section 4.3.3).

Unlike Np, Pu can exist in several oxidation states under ambient groundwater conditions. While it has been shown that Pu(IV) added to a solution will eventually oxidize such that the dominant aqueous species becomes Pu(V), Pu can occur simultaneously in the +3, +4, +5, and +6 oxidation states (Duff et al., 1999). Each valence state exhibits different solubility and mobility behavior (Duff et al., 1999), but the more-oxidized forms are typically more soluble (Shaughnessy et al., 2003). Several researchers have noted a change in the oxidation state of Pu following mineral contact. In some cases Pu (VI) was reported to reduce to Pu(IV) following contact with δMnO_2 (Shaughnessy et al., 2003), while others have reported the disproportionation of Pu(V) to Pu(VI) and Pu(IV) (Keeney-Kennicutt and Morse, 1985). The results of Shaughnessy et al. (2003) were based on EXAFS analysis of solid samples, which is a less-invasive technique than the solvent extraction method used by Keeney-Kennicutt and Morse (1985). However, both techniques may contribute to redox changes. Redox changes due to x-ray beam damage has been observed in some EXAFS studies (e.g. Zavarin, 1999). The solvent extraction process may also be problematic for evaluating the oxidation state of sorbed Pu since the samples need to be pre-treated, typically with acid, to desorb the Pu prior to solvent extraction. Thus, the results of our solvent extractions should be interpreted with caution. The Pu oxidation state in our sorption experiments is discussed in Section 4.4.3.

Based on the solution composition of our sorption experiments, carbonate complexes of Pu(IV) and Np(V) are expected to dominate at high pH (Figure 5). At the low pH, the two radionuclides are dominated by oxide and hydroxide species. From pH 3 to 7, NpO_2^+ is the dominant Np(V) species while Pu(IV) forms a series of hydroxide species in this same pH range.

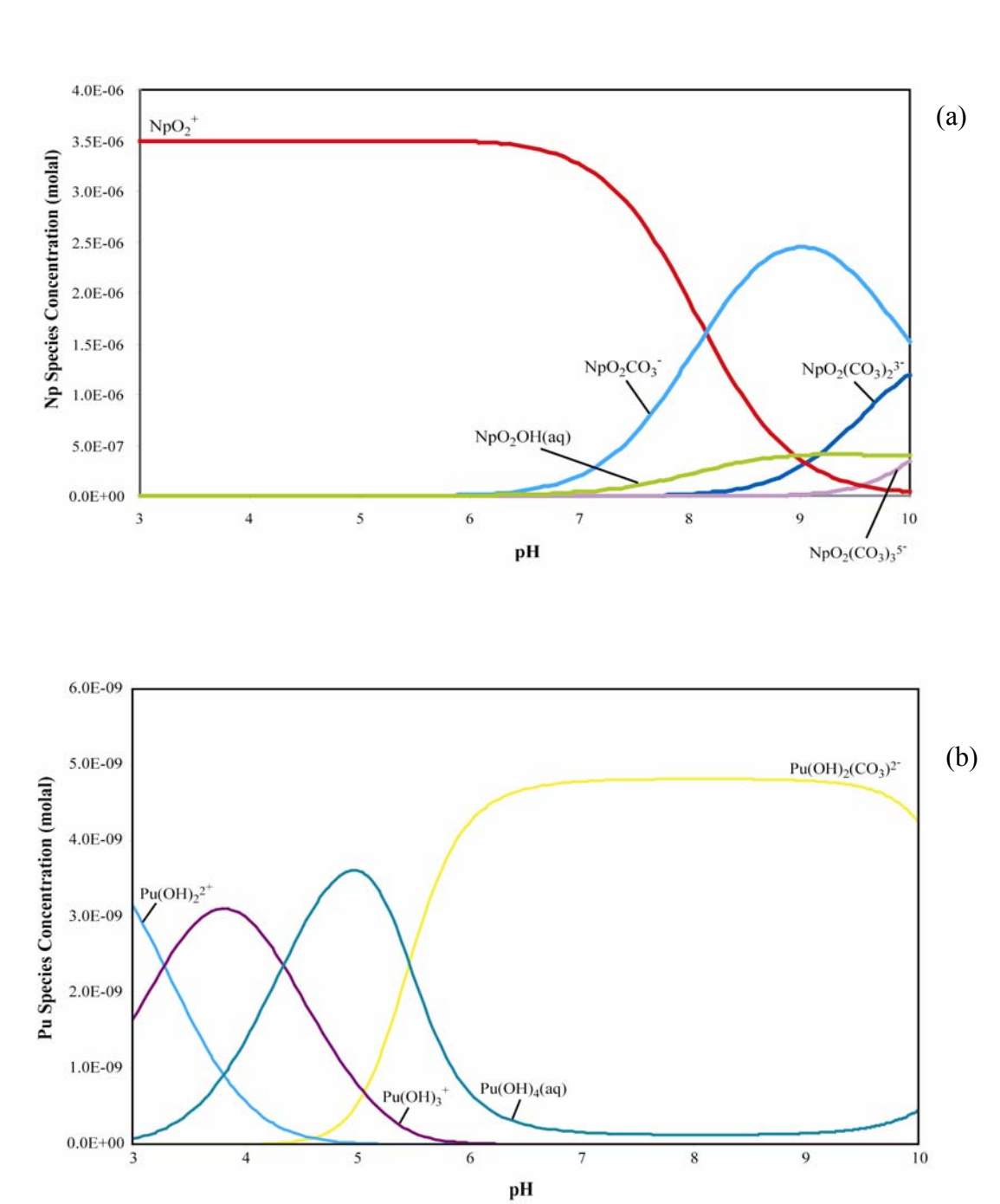

Figure 5. Aqueous speciation of (a) Np(V) and (b) Pu(IV) as a function of pH given the sorption experiment solution conditions.

In addition to aqueous speciation, the Mn oxide surface will undergo changes in surface speciation. Figure 6 shows the predicted surface speciation of birnessite based on the diffuse double layer model reaction constants of Tonkin et al. (2004) and the aqueous solution composition in the Np(V)-birnessite sorption experiment (details regarding this model are reported in Section 4.3.4)[5]. At low pH, the surface becomes less negatively charged. However, the charge on the birnessite surface remains negative over the entire pH range examined in our experiments. Above pH ~7, sorbed Mn(II) nearly saturates one of the two surface site types (the >XOH site) on the birnessite surface. The total percentage of available surface sites occupied by the background cations increases linearly from only 1.65% at the lowest pH to 61.4% at the highest pH. Interestingly, the modeled divalent cations only sorb to the >XOH site type.

The model of Appelo and Postma (1999) predicts similar, but not identical, surface speciation (Figure 7). As in the previous model, Mn^{2+} is the dominant sorber. However, unlike the Tonkin et al. (2004) model, Na^{+} outcompetes Ca^{2+} and Mg^{2+} for surface sites at low pH. Since the Tonkin model only addresses the sorption of divalent cations, predicted Na^{+} sorption cannot be compared. Interestingly, due to the strong sorption of Mn^{2+} at low pH, the surface is predicted to be positively charged below pH 6. Differences between the two models illustrate how model predictions are dependent on our description of the Mn oxide surface, the associated surface complexation model, and the data used to calibrate the model. Because the Tonkin model focused on the sorption of divalent cations while the Appelo and Postma model accounted for both divalent and monovalent cations, we would expect some significant differences in our modeling results. Nevertheless, both models predict that sorbed Mn^{2+} will dominate the birnessite surface.

4.2 Mn Oxide Mineral Characteristics

In addition to the XRD analysis used to identify the crystallographic phase of each manganese oxide (see Section 3.1), images of the mineral surfaces were made using Scanning Electron Microscopy (SEM), and surface areas were measured on a Micromeritics Gemini II 2370 surface area analyzer using multipoint Brunauer-Emmett-Teller (BET)-N_2 adsorption.

According to the SEM images (Figures 8a and 8b), the framework mineral pyrolusite exhibits a bimodal size distribution with smaller fragments ranging from 0.1-0.5 μm and larger fragments ranging from 1-5 μm. Birnessite (Figures 8c and 8d), a layered mineral, primarily occurs as 5-20 μm aggregates of .5-2 μm bladed-to-platy crystals, although there is some finer grained material present. SEM images of cryptomelane (Figures 8e and 8f), indicate that this tunnel-structure mineral formed as 0.1-0.5 μm needles or plates that cluster into 1-10 μm aggregates.

[5] In this report, we describe surface complexation only on the birnessite surface. Surface complexation models for the cryptomelane and pyrolusite surfaces were not available in the literature at the time this report was prepared.

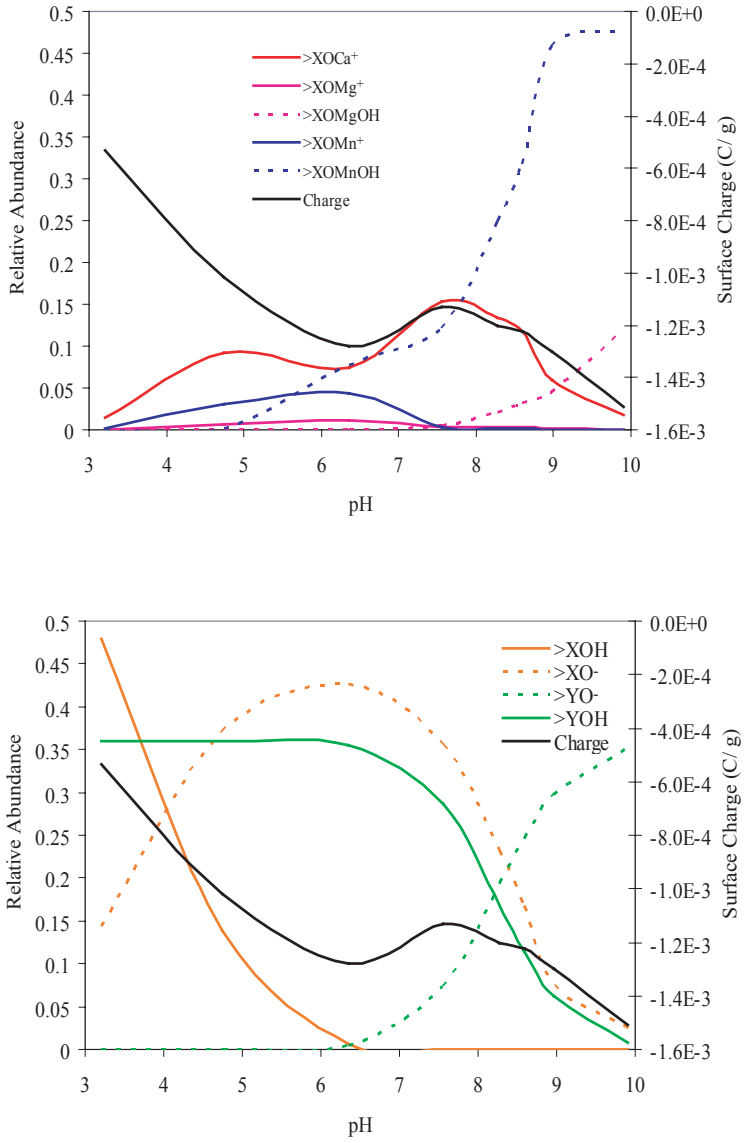

Figure 6. Surface speciation of birnessite based on the model of Tonkin et al. (2004) and water chemistry from the Np-birnessite sorption experiment. Species concentration (left axis) and surface charge (right axis).

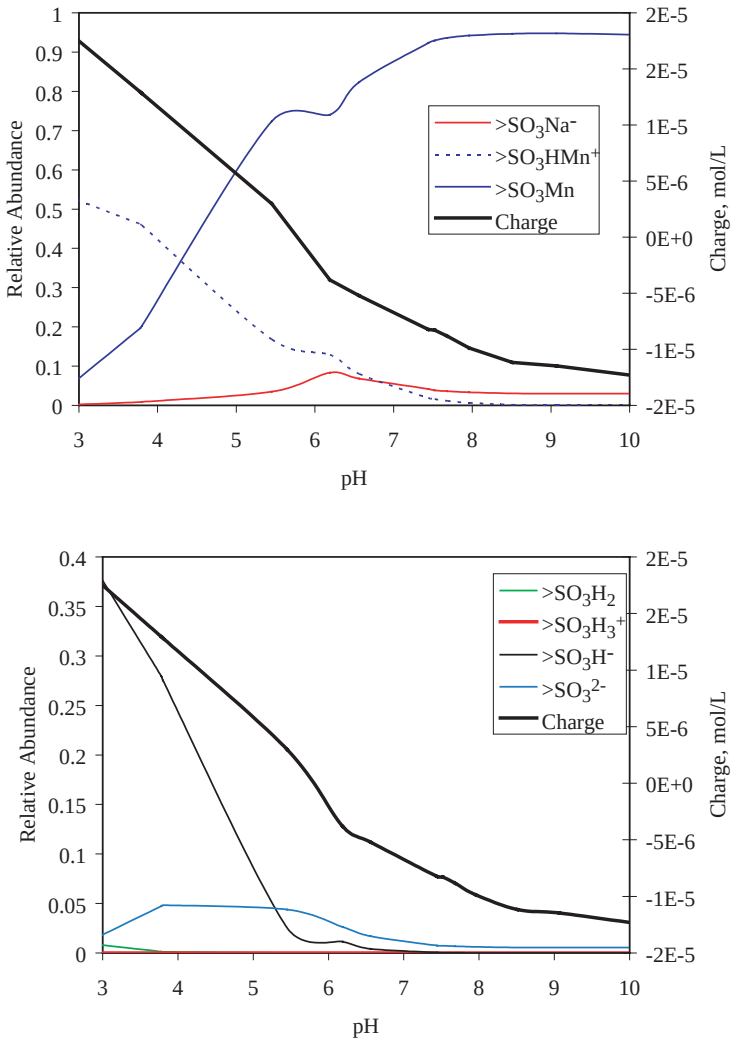

Figure 7. Surface speciation of birnessite (dominant species only) based on the model of Appelo and Postma (1999) and water chemistry from the Np-birnessite sorption experiment. Species concentrations (left axis) and surface charge (right axis).

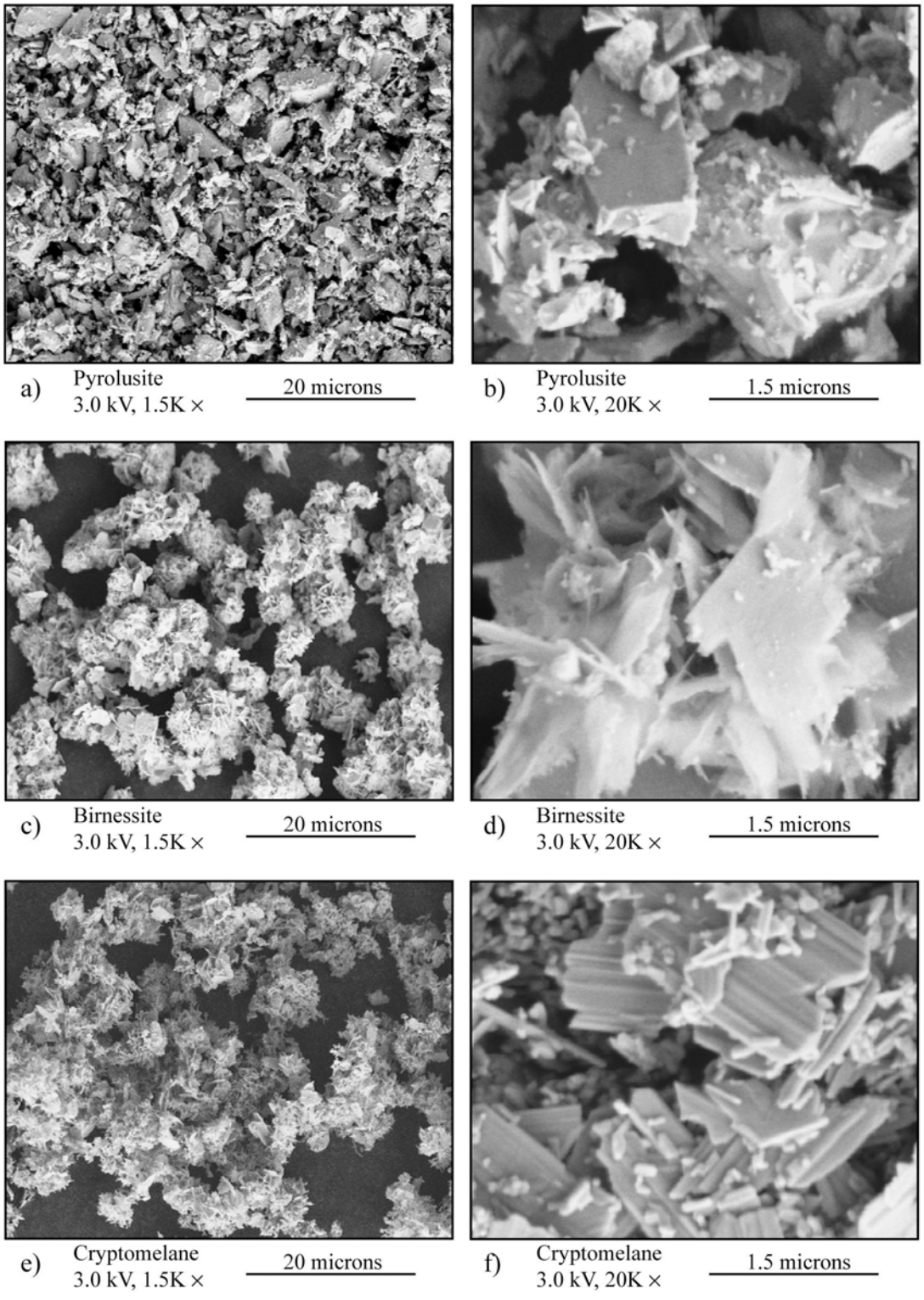

Figure 8. SEM images of the three manganese oxide minerals. Images on the left are magnified by 1500x; images on the right are magnified by 20,000x.

Table 2 summarizes the surface areas measured for each mineral. Note that the surface area estimates of the birnessite and the cryptomelane for the Np(V) and Pu(IV) experiments are different. The two cryptomelane values are within the analytical error; however, the birnessite values are significantly different. The lower surface area of the birnessite used in the Np experiments resulted from the additional mineral rinsing described in Section 3.1.

Table 2. Mineral surface areas

	Np	Pu
Pyrolusite, m^2/g	2.30 +/- 0.04	2.30 +/- 0.04
Birnessite, m^2/g	41.36 +/- 0.08	54.70 +/- 0.13
Cryptomelane, m^2/g	11.79 +/- 0.15	10.54 +/- 0.78

Although the additional rinsing of the birnessite reduced the measured surface area of birnessite, it is unlikely that it affected the stability of the mineral since rinsing was accomplished at near neutral pH. However, the stability of all three minerals at the low pHs used in sorption experiments is questionable. In all six experiments, major cation concentrations in the sorption solutions were measured after one month. The concentration of aqueous Mn^{2+} increased dramatically with decreasing pH, regardless of which mineral was used (Figure 9). Modeling[6] the solubility of pyrolusite (Figure 9a), birnessite (Figure 9b), and cryptomelane (Figure 9c) in contact with batch sorption solutions indicates that the increase in aqueous Mn^{2+} measured in the lower pH solutions could be, in part, the result of mineral dissolution. However, the stability of the Mn oxide minerals would be compromised significantly at low pH only if the redox state of solutions decreased from equilibrium with the atmosphere to a lower Eh (i.e an $O_2(g)$ fugacity of $\sim 10^{-5}$ bar.).

Although the mineral solubility models can qualitatively explain the aqueous Mn^{2+} concentration at pH 3, they do not accurately follow the measured changes in Mn^{2+} concentrations as a function of pH. For instance, there is a small amount of Mn^{2+} present at the highest pH that is not predicted by our model. Furthermore, aqueous Mn^{2+} increases steadily with decreasing solution pH starting at approximately pH 7.5 for all three minerals. The mineral solubility model suggests that aqueous Mn^{2+} should increase exponentially with decreasing pH at a much lower pH (pH 3.2 – 5.5, depending on which mineral and which oxygen fugacity are assumed).

[6] Modeling of the pyrolusite and birnessite dissolution at various oxygen fugacities was accomplished using the REACT program in the Geochemist's Workbench software suite (Bethke, 2002) in conjunction with the GEMBOCHS Datacom.V8.R6 thermodynamic database (Johnson and Lundeen, 1997). Modeling the cryptomelane dissolution was accomplished using the mineral solubility equation provided by Parc et al. (1989).

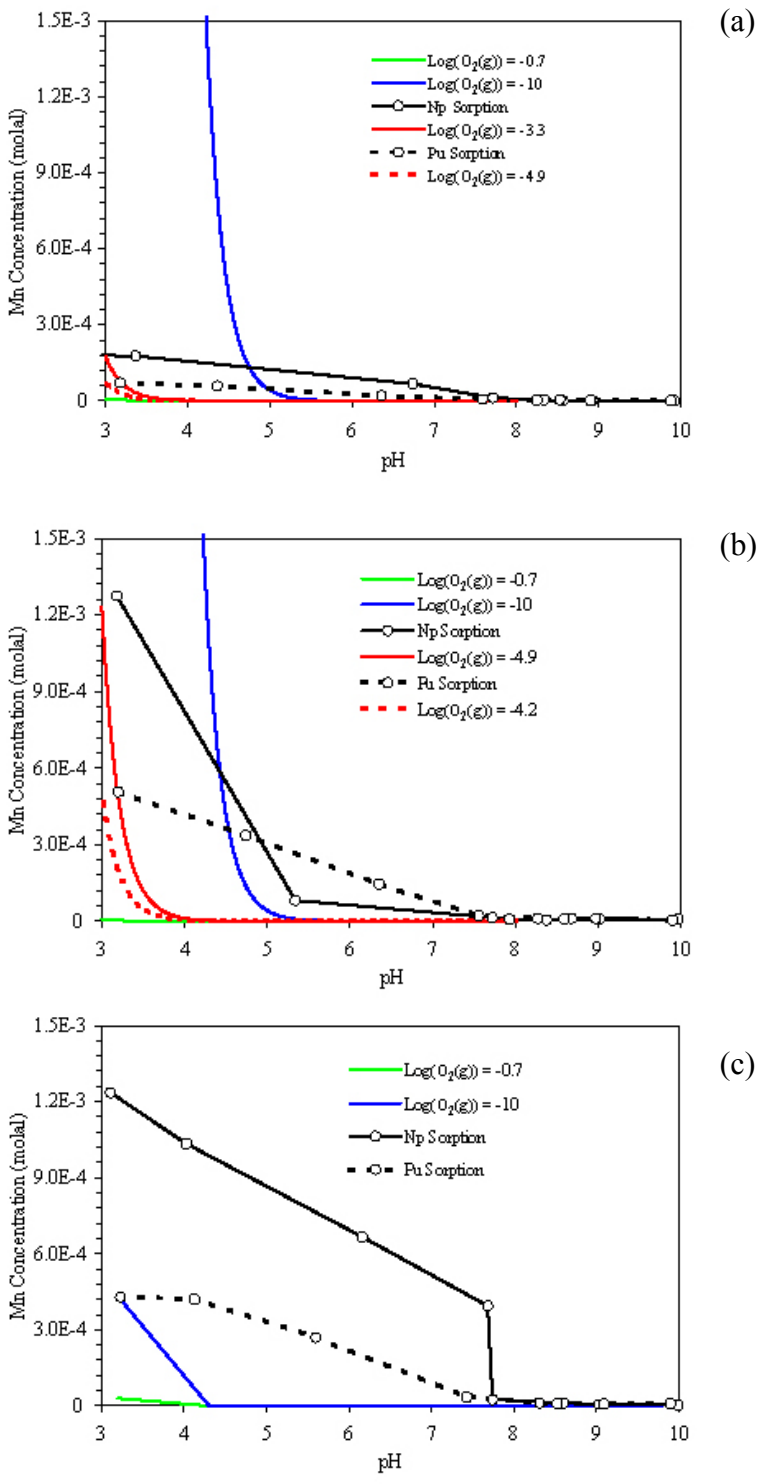

Figure 9. Mn^{2+} concentrations in Np (—o—) and Pu (· -o- ·) sorption experiments with (a) pyrolusite, (b) birnessite, and (c) cryptomelane, predicted Mn^{2+} concentrations at $Log(O_2(g)) = -0.7$ (—) and $Log(O_2(g)) = -10$ (—), and $O_2(g)$ fugacity consistent with measured Mn^{2+} concentrations at pH 3 (Np (—) and Pu (· - -)).

A second source of Mn^{2+} in sorption solutions may be cation desorption from mineral surfaces: if Mn^{2+} remained sorbed to the surface after mineral synthesis, it could be released during sorption experiments. The effect is illustrated in Figure 10 which shows the *predicted* change in aqueous and sorbed Mn^{2+} as a function of pH based on the surface complexation model of Tonkin et al. (2004). The model suggests that a fraction of the Mn^{2+} observed at low pH may be the result of its desorption from surface sites.

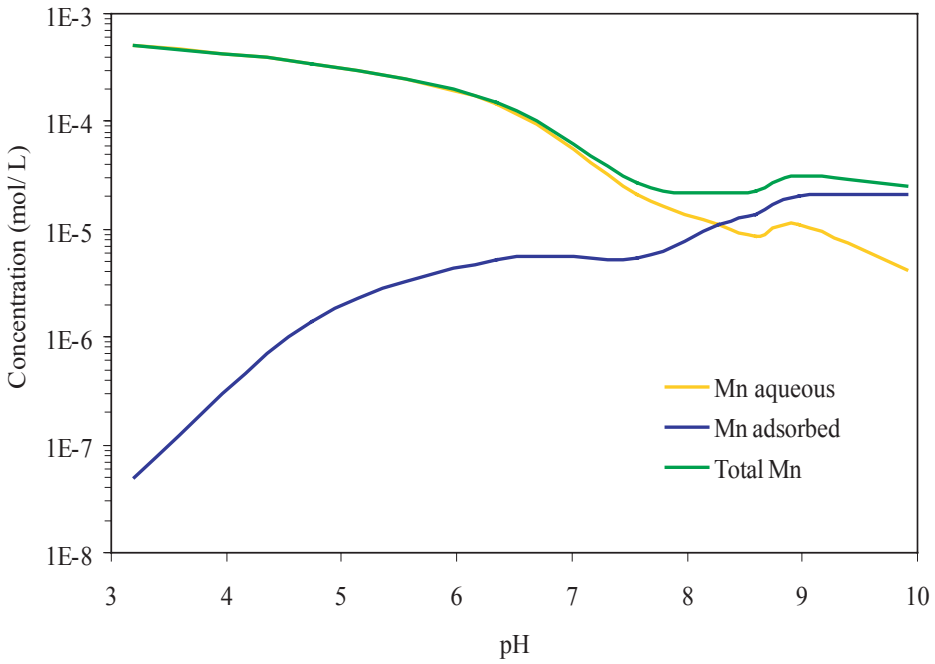

Figure 10. Predicted aqueous, total, and sorbed Mn^{2+} as a result of surface complexation using the Tonkin diffuse double layer model (Tonkin et al., 2004).

4.3 Np(V) Sorption and Desorption Experiments

4.3.1 Np Sorption Data

The sorption of Np was examined using three different manganese oxide minerals for about four weeks. Data from these experiments are reported in Table A-1 of the Appendix. Figure 11 presents Np sorption onto three manganese oxides, as functions of pH and time. In general, the sorption of Np onto all three minerals increased from zero or a few percent at pH 3 to ~63% at around pH 8.2, and then reached a plateau at higher pH. The sorption behavior between pH ~3-8.2 indicates that pH greatly affects Np sorption. Furthermore, the sorption of Np appears to correlated with the abundance of $NpO_2OH_{(aq)}$ in solution (Figure 5). The plateau in sorption at high pH may be the result of aqueous Np-carbonate complexation which also results in a decrease in the abundance of $NpO_2OH_{(aq)}$. Our data show that the rates of Np sorption are initially fast (<1 day). However a small amount of Np continues to sorb over the 30 day sorption time period. This two-step sorption behavior is commonly observed in batch sorption experiments.

Np(V) sorbed only moderately (up to ~60%) at pH 8. Figure 12 compares sorption data obtained after one month for Np sorption onto the different minerals as a function of pH. Interestingly, sorption of Np(V) to all three minerals is comparable when examined in terms of % Np sorbed. However, if sorption is evaluated on a surface area basis, sorption to the birnessite surface is much weaker than for cryptomelane and pyrolusite. The calculated K_ds from sorption experiments are plotted in Figure 13. The K_d values range from <100 mL g^{-1} at lower pH to >1000 mL g^{-1} at higher pH. The high-pH K_ds are in agreement with the values reported by Keeney-Kennicutt and Morse (1984) for synthetic MnO_2 in deionized water and seawater (16000 and 4600 mL/g, respectively) when the order-of-magnitude difference in surface area is accounted for (348 m^2/g versus 41.4 m^2/g in our birnessite experiments). These values also agree with the K_d reported in Kersting and Reimus (2003) (Figure 1). However, our data quantify the pH-dependence and clearly show that pH will have a great effect on the sorption of Np to Mn oxides.

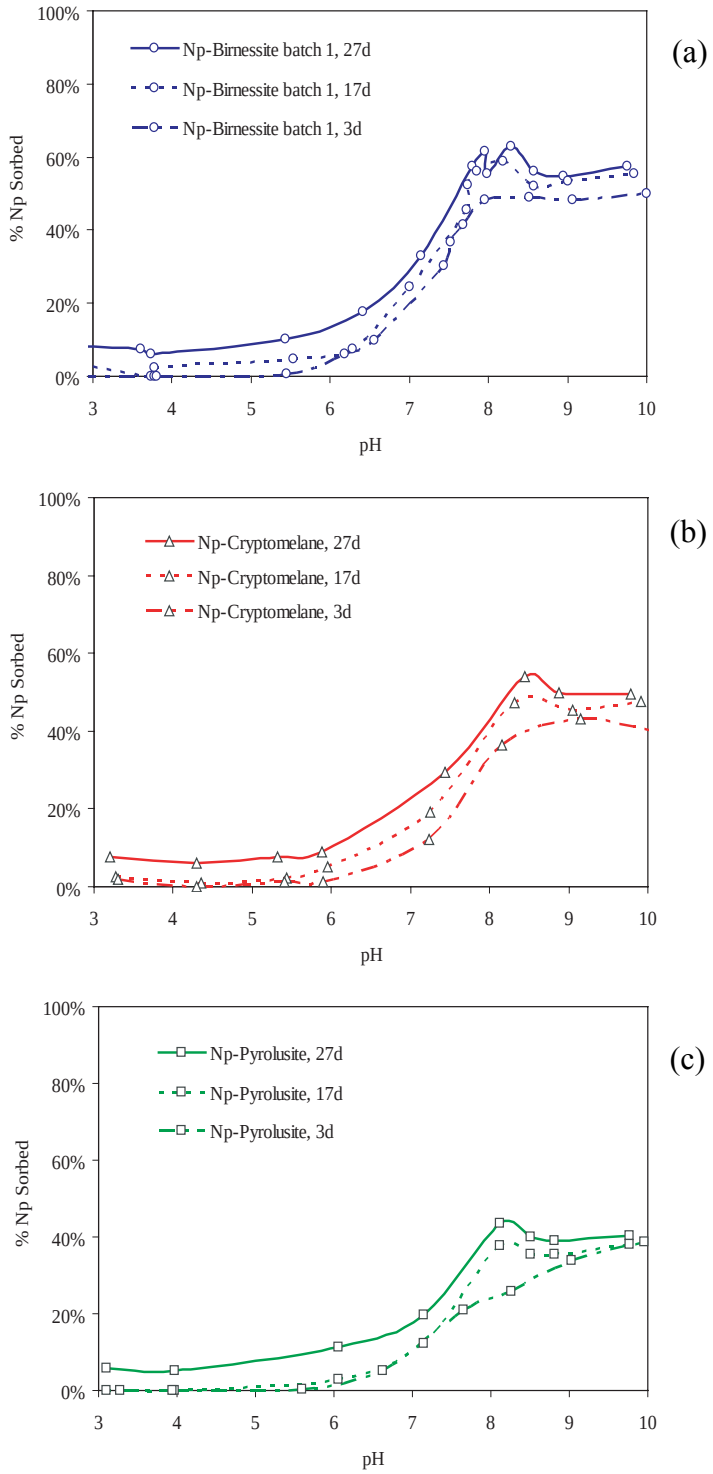

Figure 11. Np sorption to (a) birnessite, (b) cryptomelane, and (c) pyrolusite as functions of pH and time.

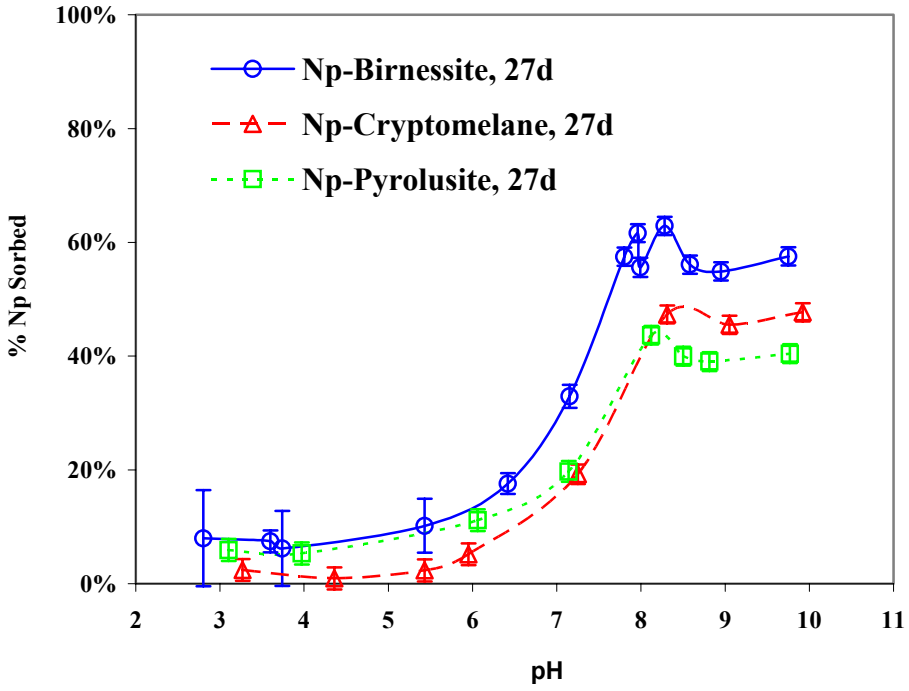

Figure 12. Comparison of Np sorption to three manganese oxides.

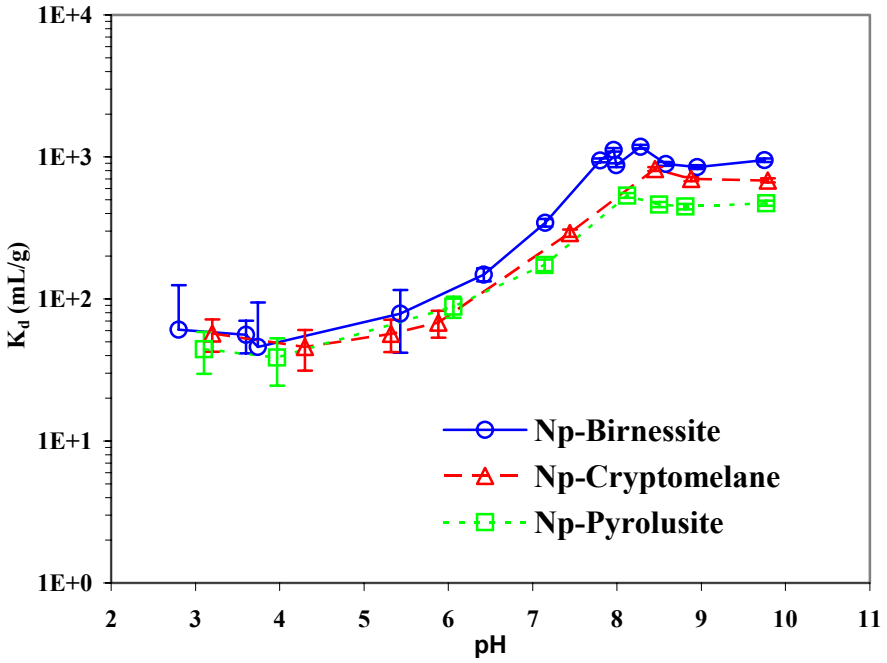

Figure 13. Np K_d versus pH at the end of the 30 day sorption experiment.

4.3.2 Np Desorption Data

In order to investigate the reversibility of Np sorption onto manganese oxides, desorption experiments were initiated at the termination of the sorption experiments. See Table A-2 in the Appendix for a summary of the data. Sorption is considered reversible if the sorption curve obtained from the desorption experiment is the same or similar to the one obtained from the sorption experiment. Since Np(V) exhibited little to no sorption at pH < 6, desorption over this pH range could not be measured. However, the desorption data above pH 7 for all three minerals show similar trends as the sorption curves (Figure 14). This suggests that desorption of Np(V) from the three manganese oxides was fast and reversible.

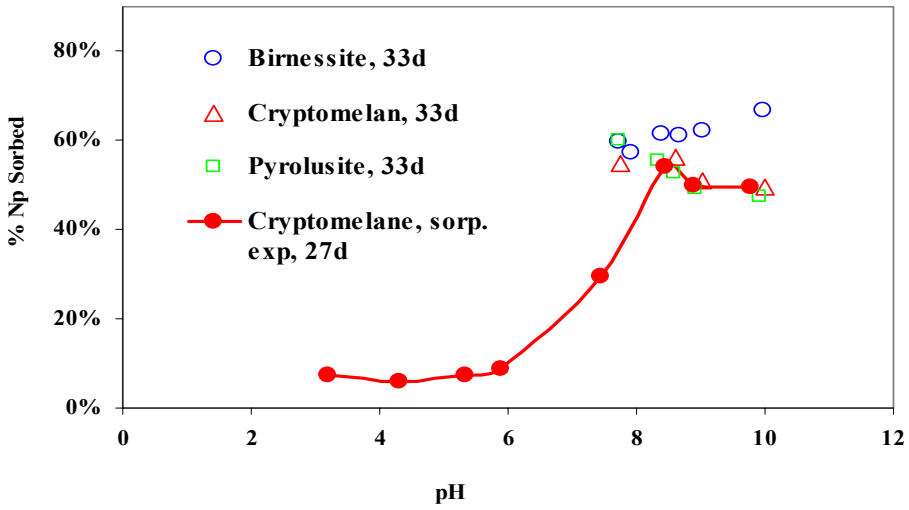

Figure 14. Comparison of Np sorption (cryptomelane, solid line) and desorption (birnessite (○), cryptomelane (△), and pyrolusite (□)) data.

4.3.3 Np Oxidation State Characterization

The oxidation states of Np species in the desorption supernatant were examined by solvent extraction using chelating reagents PMBP and D2EHPA (Table 3). The results appear to indicate that in the presence of birnessite, 7%, 20% and 32% of Np at pH 4, 7 and 10 had been oxidized to Np(VI) in the desorption supernatant, respectively. This result is contrary to our general expectation that Np(V) will be the only stable aqueous species in solution under ambient conditions. The mechanism of oxidation remains unclear at this time, and further investigation would be necessary to confirm this result. There was no significant change in the oxidation state of Np in contact with cryptomelane and pyrolusite.

Table 3. Np oxidation state in supernatant measured by solvent extraction.

		Percentage of Np oxidation state		
		4+	5+	6+
Birnessite	pH4	1%	92%	7%
	pH7		80%	20%
	pH10		68%	32%
Cryptomelane	pH4	3%	96%	1%
	pH7	1%	97%	2%
	pH10		99%	1%
Pyrolusite	pH4		98%	2%
	pH10		99%	1%

4.3.4 Np Data Modeling

The Np sorption data were modeled by applying the diffuse double layer model of Tonkin et al. (2004) to the 1-day sorption data for Np on birnessite.[7] The sorption model accounted for changes in the major cation solution composition as a function of pH (data reported in Table A-3 of the Appendix) and sorption of these species to the birnessite surface along with Np. The Tonkin model is based on a two-site model (>XOH and >YOH) with α >XOH sites and 1-α >YOH sites. Based on a number of acid-base titrations, Tonkin estimated α to be 0.64. The reactive site density used in our model was based on the theoretical value of 2.8 μmol/m^2. This is close to the total site density used by Dzombak and Morel (1990) for high surface area iron oxide (3.8 μmol/m^2). Aqueous speciation reaction constants were taken from speciation data reported in Zavarin and Bruton (2004a; 2004b); surface complexation reaction constants for major cations were taken directly from Tonkin et al. (2004). These data are reported in Table 4. Interestingly, Ca^{2+}, Mg^{2+}, and Mn^{2+} sorption occurs only on the >XOH site which has a very low pKa (very low acid dissociation constant). This is described by Tonkin et al. (2004) as the strong sorption site. It should also be noted that the Tonkin model does not include sorption of monovalent cations such as Na^+ and K^+.

The one-site model of Appelo and Postma (1999) includes surface complexation of Na^+ and K^+ as well as Ca^{2+}, Mg^{2+} and Mn^{2+}; under our experimental conditions, their model predicts, as does the Tonkin model, that Mn^{2+} will dominate on the surface. The Appelo and Postma model was used to fit our Np sorption data as well; like the Tonkin model, a two-species surface complexation model resulted in the best fit to the data, as will be described below. Major cation and acidity reaction constants for the Appelo and Postma model are reported in Table 4.

[7] Surface complexation to cryptomelane and pyrolusite was not attempted because a model was not available in the literature.

Table 4. Reaction constants used in FITEQL surface complexation model.

Reaction*	Log K
Dominant Aqueous Species	
$H^+ + OH^- = H_2O$	14.0
$NpO_2^+ + H2O = NpO_2OH + H^+$	-8.90
$NpO_2^+ + HCO_3^- = NpO_2CO_3^- + H^+$	-5.73
$NpO_2^+ + 2\ HCO_3^- = NpO_2(CO_3)^{3-} + 2\ H^+$	-13.66
$NpO_2^+ + 3\ HCO_3^- = NpO_2(CO_3)_3^{5-} + 3\ H^+$	-22.49
$HCO_3^- + H^+ = H_2CO_3(aq)$	6.34
$HCO_3^- = CO_3^2- + H^+$	-10.33
Tonkin Model Surface Reactions	
$>XOH = >XO^- + H^+$	-2.35
$>YOH = >YO^- + H^+$	-6.06
$>XOH + Ca^{2+} = >XOCa^+ + H^+$	-1.50
$>XOH + Mg^{2+} = >XOMg^+ + H^+$	-2.40
$>XOH + Mg^{2+} + H2O = >XOMgOH + 2\ H^+$	-7.70
$>XOH + Mn^{2+} = >XOMn^+ + H^+$	1.20
$>XOH + Mn^{2+} + H2O = >XOMnOH + 2\ H^+$	-2.70
Appelo and Postma Model Surface Reactions	
$>SO_3H_2 + H^+ = >SO_3H_3^+$	1.84
$> SO_3H_2 = >SO_3H^- + H^+$	-2.41
$> SO_3H_2 = >SO_3^{2-} + 2\ H^+$	-7.95
$> SO_3H_2 + H^+ + Cl^- = >SO_3H_3Cl$	3.28
$> SO_3H_2 + Na^+ = >SO_3HNa + H^+$	-1.41
$> SO_3H_2 + Na^+ = >SO_3Na^- + 2\ H^+$	-5.92
$> SO_3H_2 + K^+ = >SO_3HK + H^+$	-0.71
$> SO_3H_2 + K^+ = >SO_3K^- + 2\ H^+$	-5.22
$> SO_3H_2 + Ca^{2+} = >SO_3HCa^+ + H^+$	-0.01
$> SO_3H_2 + Ca^{2+} = >SO_3Ca + 2\ H^+$	-5.09
$> SO_3H_2 + Mg^{2+} = >SO_3HMg^+ + H^+$	-0.6
$> SO_3H_2 + Mg^{2+} = >SO_3Mg + 2\ H^+$	-5.51
$> SO_3H_2 + Mn^{2+} = >SO_3HMn^+ + H^+$	3.17
$> SO_3H_2 + Mn^{2+} = >SO_3Mn + 2\ H^+$	-1.97

* Birnessite reactive site density is 2.8E-6 mol/m^2. Fraction of >XOH sites is 0.64 for the Tonkin model.

The surface complexation modeling results based on the Tonkin model are shown in Figure 15 and summarized in Table 5. Figure 15a presents data fits using a single Np surface species. While no single species fits the sorption data well, the results suggest that Np sorption is best modeled as surface complexation to the >YOH surface site. The Np sorption edge (pH 6 to 8) correlates with the pKa of the >YOH site; Np sorption increases as the surface >YOH site deprotonates. The poor fits using a single-species suggest that at least two surface species are necessary to adequately fit our data.

Figure 15b presents data fits using two Np surface species. Surface complexation models using two aqueous Np species provide a much better, particularly at the sorption plateau in the alkaline range. Note from Table 5 that the two species models have much lower WSOS/ DF values, indicating that the two species models statistically are a better fit to the data. The best fit using the Tonkin model was achieved with a Np oxide and hydroxide surface species.

The experience with modeling Np sorption using the Appelo and Postma model was similar (Figure 16). With this approach, a single surface species was unable to fit all the data while a two-species model fit the data quite well. As in the Tonkin model, the best fit was achieved with a Np oxide and hydroxide species. Best-fit reaction constants using two species are reported in Table 5.

All of the models described above more accurately fit the data below pH 8 than above pH 8. Several factors could account for the lack of model fit. The disparity could be related to uncertainty in the aqueous Np-carbonate complexation that occurs at these higher pHs. Uncertainty in other model parameters and the sorption data itself could be affecting the model fits as well. We chose to minimize the number of fitting parameters by only varying Np surface complexation constants. The surface complexation model includes both protonation and deprotonation reaction constants and surface complexation constants for the major cations in solution. If all protonation, deprotonation, and surface complexation reaction constants were allowed to vary, our model could certainly fit the data more precisely. However, it would result in a fitting exercise that could no longer be related directly to the surface complexation models of Appelo and Postma (1999) and Tonkin et al. (2004).

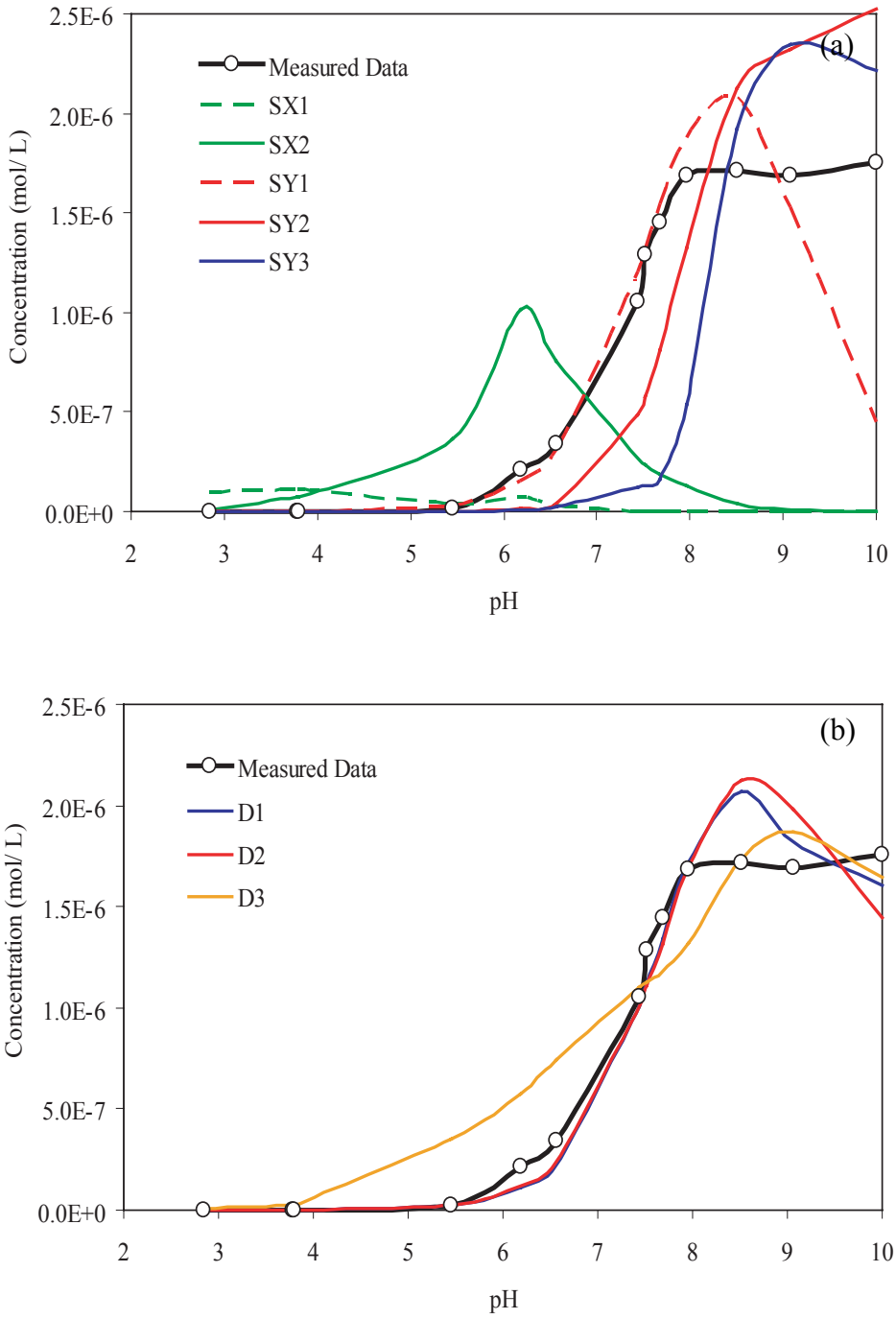

Figure 15. Model fits to Np sorption data based on the diffuse double layer model of Tonkin et al. (2004). (a) single surface species, (b) two surface species. Data and model fits reported as mol L^{-1} sorbed. Model names are explained in Table 5.

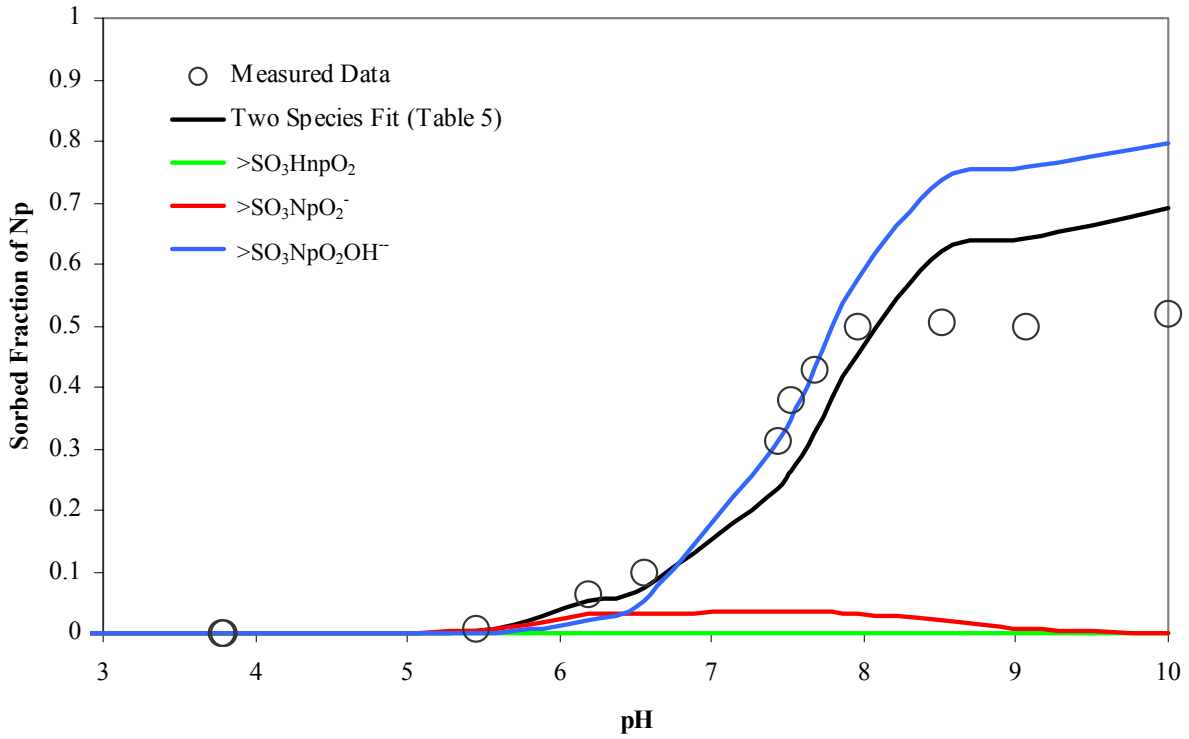

Figure 16. Model fits to Np sorption data based on the diffuse double layer model of Appelo and Postma (1999) using single surface species (green, red, blue) and two surface species (black).

Table 5. Np surface complexation reaction constants.

	Model Name	Reaction	Log K	WSOS/ DF[1]
		Tonkin Model Results		
Single Species	SX1	$>XOH + NpO_2^+ = >XONpO_2 + H^+$	0.71	1.35
	SX2	$>XOH + NpO_2^+ + H_2O = >XONpO_2OH^- + 2H^+$	-3.36	1.25
	SY1	$>YOH + NpO_2^+ = >YONpO_2 + H^+$	-3.21	0.16
	SY2	$>YOH + NpO_2^+ + H_2O = >YONpO_2OH^- + 2H^+$	-9.66	0.22
	SY3	$>YOH + NpO_2^+ + HCO_3^- = >YONpO_2CO_3^{2-} + 2H^+$	-4.57	0.49
Two Species	D1	$>YOH + NpO_2^+ = >YONpO_2 + H^+$	-3.38	0.02
		$>YOH + NpO_2^+ + H_2O = >YONpO_2OH^- + 2H^+$	-10.23	
	D2	$>YOH + NpO_2^+ = >YONpO_2 + H^+$	-3.34	0.04
		$>YOH + NpO_2^+ + HCO_3^- = >YONpO_2CO_3^{2-} + 2H^+$	-5.07	
	D3	$>YOH + NpO_2^+ + H_2O = >YONpO_2OH^- + 2H^+$	-1.77	0.06
		$>YOH + NpO_2^+ + HCO_3^- = >YONpO_2CO_3^{2-} + 2H^+$	-4.90	
		Appelo and Postma Model Results		
		$>SO_3H_2 + NpO_2^+ = >SO_3NpO_2^- + 2\ H^+$	-4.55	62[2]
		$>SO_3H_2 + NpO_2^+ + H_2O = >SO_3NpO_2OH^{2-} + 3\ H^+$	-11.34	

[1] WSOS/ DF is the ratio of the Weighted Sum of the Squares and the loss of Degrees of Freedom. It is a measure of the goodness of fit between the model and the measured data, and can be used to compare the fits of two different models.
[2] Data fit achieved using a slightly different version of the FITEQL code which calculates WSOS/DF differently.

4.4 Pu Sorption and Desorption Experiments

4.4.1 Pu Sorption Data

Batch Pu(IV) sorption onto three different manganese oxides was measured over approximately one month. The data from these experiments are reported in Table A-4 of the Appendix. Figure 17 presents Pu(IV) sorption onto the manganese oxides as functions of pH and time. In general, Pu(IV) sorbed very little at pH 3 but increased to ~100% as the pH increased to 4.5 (pyrolusite) or 6 (birnessite and cryptomelane). Sorption remained high up to pH 8, but beyond pH 8 it decreased slightly for birnessite, significantly for pyrolusite, and negligibly for cryptomelane. As expected, pH played an important role in Pu(IV) sorption. Given the elevated carbonate concentrations at high pH (see Table A-6 in the Appendix), Pu(IV) was expected to form soluble carbonate complex species resulting in a decrease in Pu sorption. This was observed for both birnessite and pyrolusite (Figure 18). In the case of cryptomelane, Pu sorption may have

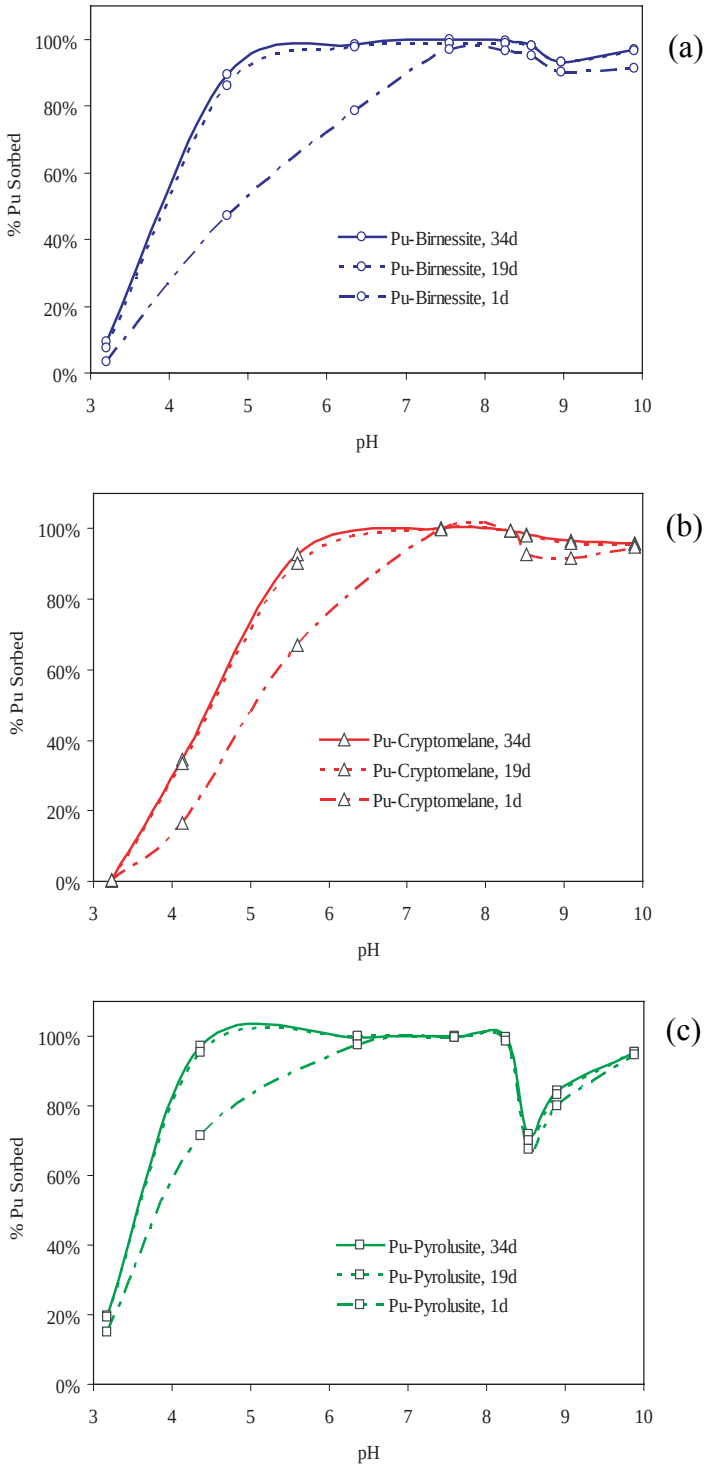

Figure 17. Pu sorption to (a) birnessite, (b) cryptomelane, and (c) pyrolusite as functions of pH and time.

been strong enough to overcome any carbonate complexation effects. Data in Figure 17 also suggest that the rate of Pu sorption is significantly slower at low pH. As will be described in the following section, these differences in sorption rates may result from significant oxidation state changes that occurred for Pu(IV) in the presence of Mn oxides.

When comparing the sorption behavior on the three minerals (Figure 19) as a function of pH, we find that all three minerals behave similarly. However, Pu sorbs to pyrolusite more strongly at low pH and more weakly at high pH than to the other two minerals. The behavior does not correlate with mineral surface area, as pyrolusite has a much lower surface area than the other two minerals. Nevertheless, regardless of the mineral type, Pu(IV) sorbs very strongly.

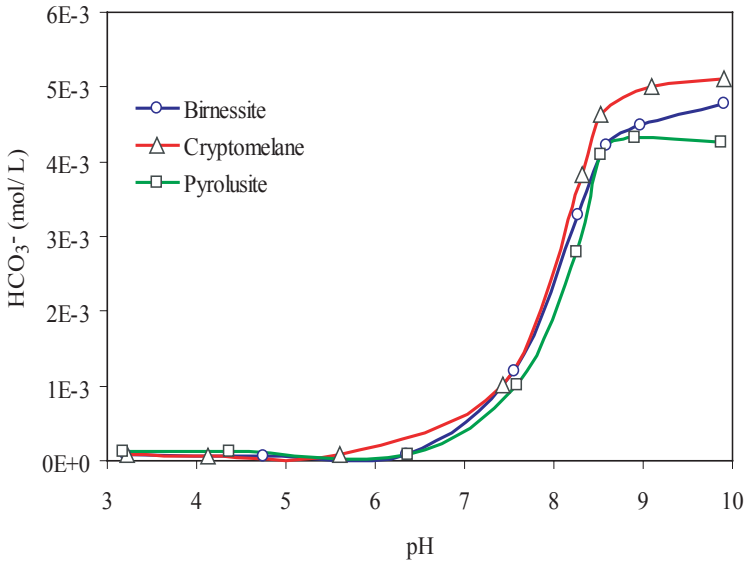

Figure 18. Bicarbonate concentrations as a function of pH for Pu sorption solutions.

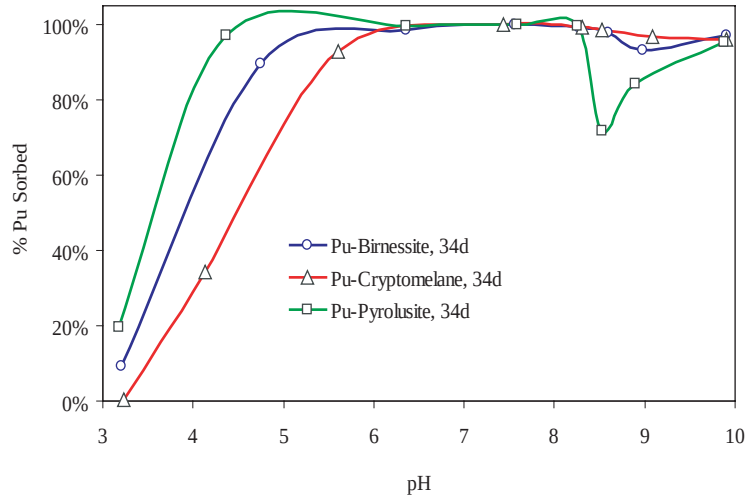

Figure 19. Comparison of Pu sorption to three manganese oxides at 34 days.

4.4.2 Pu Desorption Data

For the desorption experiment, supernatant samples were taken after 1 day, 16 days, and 22 days. The data are reported in Table A-5 of the Appendix. The amount of sorbed Pu(IV) as a function of pH and time during the desorption experiments is plotted in Figure 20. For each of the minerals examined, only minor differences in supernatant Pu concentration were measured as a function of time, indicating that desorption is very fast for all three minerals, typically reaching equilibrium in less than a day. Furthermore, the good agreement between the sorption and desorption curves (Figure 21), within experimental error, suggests that the sorption process is reversible.

The K_d values for the minerals investigated were calculated using data from the last sorption (a) and desorption (b) samples (see Figure 21a and 21b, respectively). The K_ds cover a wide range from 10^3 mL/g at pH3 up to 10^7 mL/g at pH 7. Interestingly, the decrease in Pu sorption above pH 8, presumably resulting from carbonate complexation, is more evident in the Kd plots than in the %sorbed plots (Figure 16). At neutral pH, the Pu K_d is four orders of magnitude greater than the Np K_d. The K_ds measured here are much higher than those reported by Keeney-Kennicutt and Morse (1985). Their sorption experiments were performed with Pu(V) and resulted in behavior similar to that observed for Np(V) (Keeney-Kennicutt and Morse, 1986). Our K_ds are much higher, reflecting the different Pu oxidation state used in our experiments and the fact that Pu(IV) will sorb much more effectively than Pu(V). Dyer et al. (2000a) observed a qualitatively similar pH dependence as seen here, though a direct comparison is difficult due to differences in experimental conditions. Our results clearly show that Pu sorption to manganese oxides will be an important process controlling its migration and that sorption will be dependent on the pH and carbonate alkalinity of solutions.

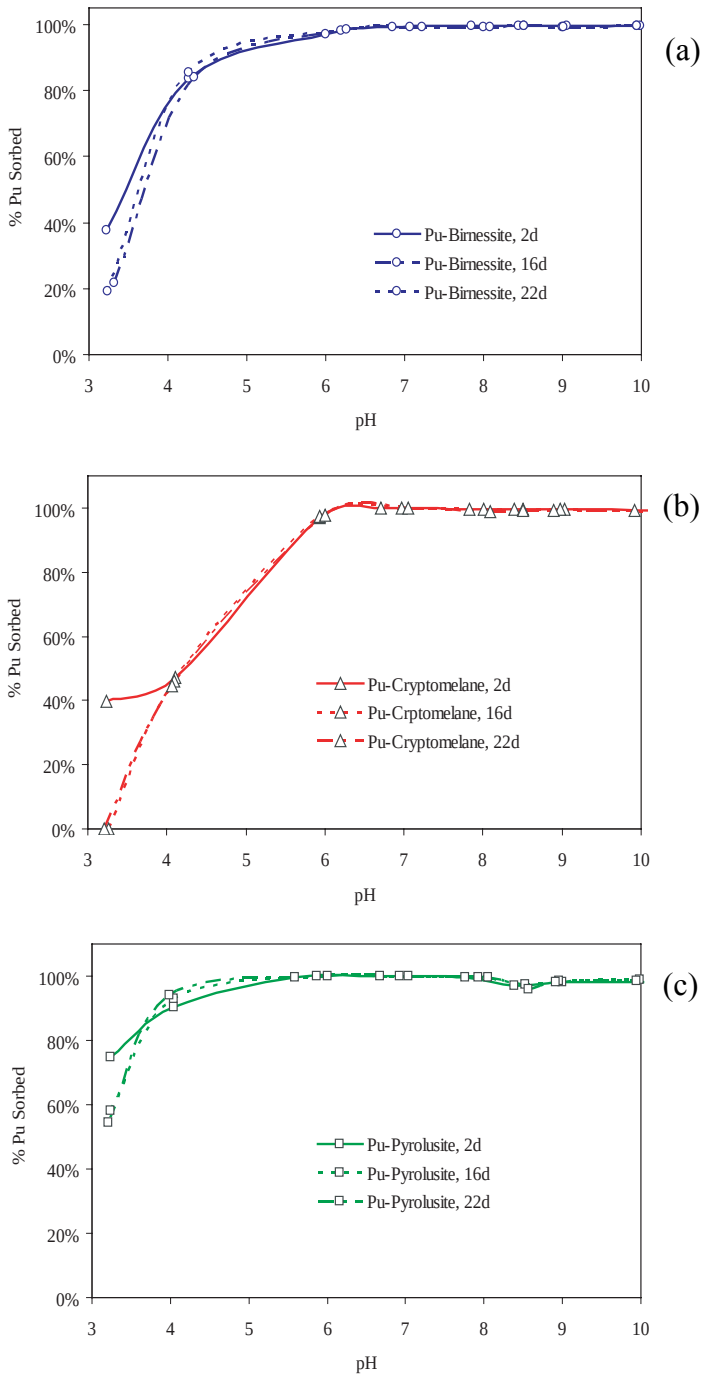

Figure 20. Pu sorption to (a) birnessite, (b) cryptomelane, and (c) pyrolusite as functions of solution pH and time in desorption experiments.

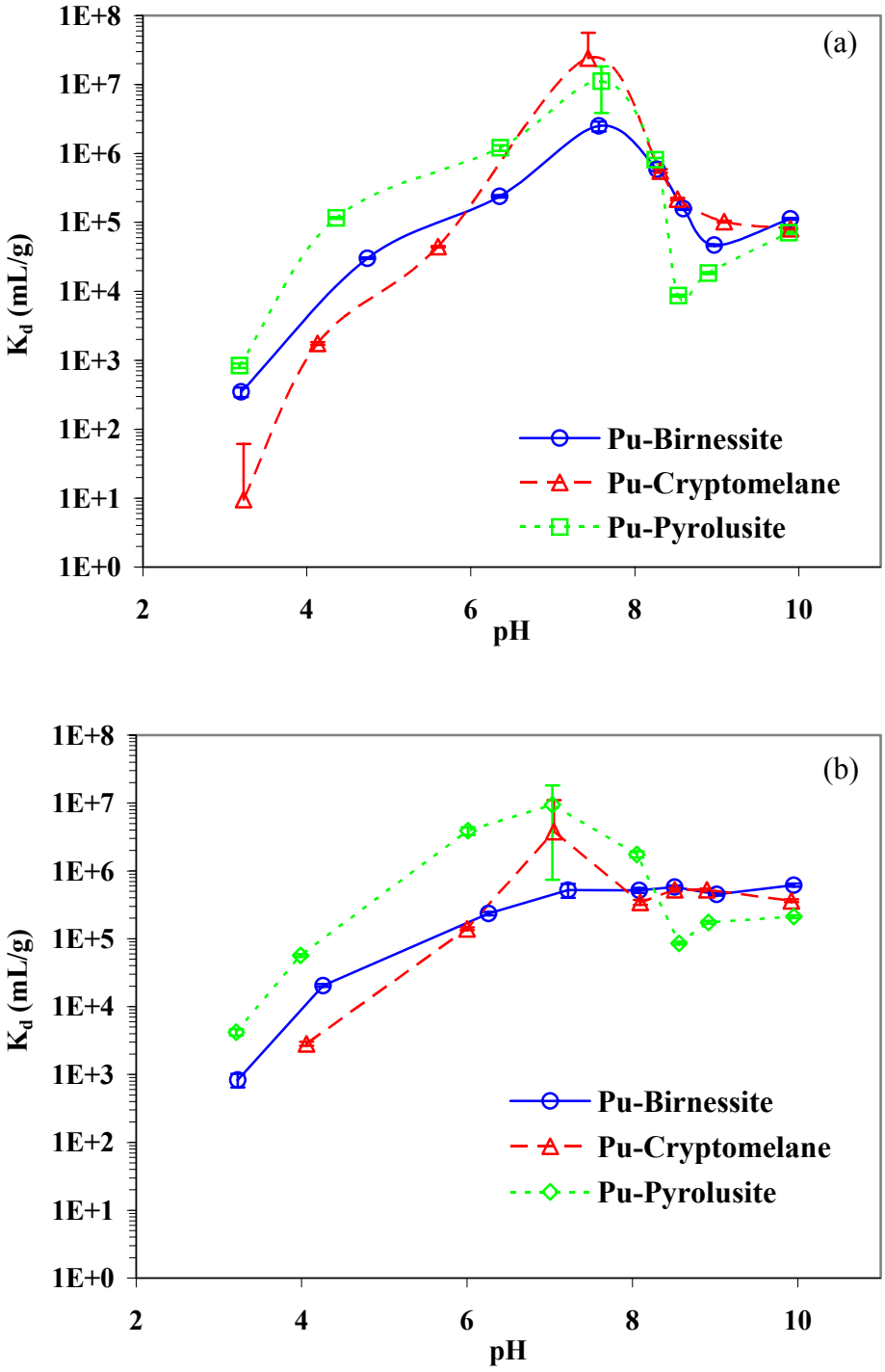

Figure 21. K_d versus pH in 30 day Pu sorption (a) and 30 day Pu desorption (b) experiments.

4.4.3 Pu Oxidation State Characterization

Plutonium ions in solution have four common oxidation states, +3, +4, +5, and +6, as species Pu^{3+}, Pu^{4+}, PuO_2^{+} and PuO_2^{2+}, respectively. Because of the spontaneous disproportionation of Pu^{4+} and PuO_2^{+} (especially PuO_2^{+}), and slow redox kinetics between PuO_2^{+}/PuO_2^{2+} and Pu^{3+}/Pu^{4+} as a result of necessary configurational changes, plutonium is the only element in the periodic table that can have all its common oxidation states coexist in the same solution at appreciable concentrations. The most common methods for characterization of plutonium oxidation states in solutions are UV/VIS spectrometry for relatively high Pu concentrations (>10^{-4} M) and solvent extraction for lower Pu concentrations. Given the experimental conditions of these sorption experiments, any Mn(III) or Mn(IV) contained in or on the manganese oxides could oxidize Pu(IV) to higher oxidation states. Solvent extraction techniques were used to characterize the plutonium oxidation states in both liquid and solid samples at the end of the desorption experiments. The end of the desorption experiments was after approximately 60 days of Pu exposure to the manganese oxide minerals. Due to the complexity of the solvent extraction process, only pH 4, 7, and 10 samples were selected and represent weakly acidic, neutral and weakly basic solution conditions.

Solvent extractions typically result in a ~2% experimental error, mostly from the liquid scintillation counting and volumetric measurements. However, some data reported here contain larger errors (~ 10-15%) due to extremely low Pu activity in sample solutions. Table 6 lists the solvent extraction results obtained from desorption experiment supernatants. The supernatant solutions were acidified but did not require any other pretreatment. The results show that at higher pH (~10) Pu(IV) remained the dominant species, although a significant amount of Pu(VI) was measured in the birnessite supernatant. Interestingly, at pH 4 ~ 99% of plutonium in the solutions was oxidized to Pu(V), Pu(VI), or both. We also found high concentration of Mn^{2+} (2 ~ 14 ppm) in the supernatant from the low pH batch solutions. It is possible that the dissolution of the Mn(IV)-oxides and reduction of Mn(IV) to Mn(II) would provide a mechanism for the oxidation of Pu(IV) to Pu(V) or Pu(VI). While this mechanism cannot be confirmed, the results indicate very clearly that Pu(IV) is likely to oxidize, predominantly to Pu(V), under slightly acidic conditions.

Table 6. Pu oxidation states in supernatant at the end of desorption experiments.

		Pu Oxidation States				colloids
		3+	4+	5+	6+	
Birnessite	pH4		1%	66%	28%	5%
	pH7**	10%	40%	10%	40%	
	pH10	1%	55%	7%	37%	
Cryptomelane	pH4			80%	19%	
Pyrolusite	pH4		1%	94%	3%	2%
	pH10		89%	2%	7%	1%

** Sample contained very low activity of Pu (< 5 cmp/mL) , so that the results were associated with errors as much as ± 10%.

At pH 7 and 10, the desorption supernatant contained very low Pu since much of the Pu had sorbed to the mineral surfaces. As a result, we attempted to measure the redox state of Pu on the mineral surface but not in the supernatant. The sorbed Pu was desorbed from the manganese oxides in 15 mL of 1N HCl and examined using solvent extraction. Table 7 shows the extraction results. It appears that Pu(VI) is dominant (>90%) in birnessite and cryptomelane samples. In pyrolusite samples, there was some Pu(III)/ Pu(IV) but a larger percentage of Pu(VI). This appears to contradict the observations of Shaughnessy et al. (2003). However, our oxidation state results may be an artifact of the desorption pretreatment process. Based on our supernatant oxidation state measurements, we find that aqueous Pu(IV) will oxidize to Pu(VI) at low pH. Since the sorbed Pu was treated with acid prior to solvent extraction, it is possible that the observed predominance of Pu(VI) results from the extraction procedure and does not represent the oxidation state of Pu on the manganese oxide mineral surface.

Table 7. Oxidation state characterization of sorbed Pu (after 1N HCl acidification).

		Pu Oxidation States				colloids
		3+	4+	5+	6+	
Birnessite	pH7			5%	94%	1%
	pH10			7%	92%	1%
Cryptomelane	pH7			9%	90%	1%
	pH10			2%	97%	1%
Pyrolusite	pH7	14%	14%		71%	1%
	pH10	9%	20%	3%	67%	1%

Given the possibility that the oxidation states of plutonium on the manganese oxides were altered during the pretreatment process, we also performed solvent extractions using Pu-sorbed minerals without the acidification pretreatment. For birnessite and pyrolusite these results (Table 8) still indicate that > 88% of the plutonium was Pu(VI). However, in contradiction to the pretreated samples (Table 7), the direct solvent extraction of plutonium showed 100% Pu(IV) on cryptomelane.

Table 8. Oxidation state characterization of sorbed Pu (Pu-manganese oxide wet pastes).

		Pu Oxidation States			
		3+	4+	5+	6+
Birnessite	pH8		7%	41%	52%
Cryptomelane	pH8		100%		
Pyrolusite	pH8		12%	13%	75%

Because the Pu oxidation state may have changed during acidification pretreatment of samples and because the efficiency of solvent extraction without acidification is not

known, these results should be interpreted with caution. Additional examination of the oxidation state of Pu in the presence of manganese oxides would be needed to better understand the redox processes at the manganese oxide surface. Given the weak sorption of Np(V) and the thermodynamic similarity of Pu(V) and Np(V) speciation, it appears unlikely that Pu(V) plays a significant role in the strong sorption of Pu on the Mn oxide surface. The oxidation state of Pu on the mineral surfaces is likely to be either Pu(IV) or Pu(VI).

5 CONCLUSIONS AND RECOMMENDATIONS

Based on the experimental results described in this report:

- Sorption of both Np(V) and Pu(IV) is strongly pH dependent
- Sorption of Np(V) and Pu(IV) to all three Mn oxide minerals examined here was fast and reversible
- The oxidation state of Pu appeared to change during sorption experiments; additional experiments would be necessary to further elucidate its behavior
- On a mass basis, Pu (as well as Np) sorbed to the three different Mn oxide minerals similarly. On a surface area basis, sorption affinity followed the order pyrolusite>cryptomelane>birnessite for both Np and Pu
- Pu sorption K_ds were up to four orders of magnitude greater than Np
- Surface complexation modeling of Np(V) sorption to birnessite was achieved using two surface species: a Np oxide and Np oxyhydroxide species
- Pu sorption to manganese oxide minerals will have a significant impact on its transport at NTS locations where Mn oxides are present (fractured tuff environments). Np and other radionuclide transport may be significantly affected as well.

The combination of experimental data reported here and literature data reviewed in this report provides sufficient data to begin to incorporate Mn oxide sorption reactions into HST (and upscaled) models and provide less conservative estimates of radionuclide transport. Future modeling efforts need to address the role of Mn oxides in radionuclide transport, particularly for Pu and Np.

6 ACKNOWLEDGEMENTS

Funding for this investigation was provided by the Environment Restoration Division's Underground Test Area Project at the U.S. Department of Energy, National Nuclear Security Administration, Nevada Site Office. This work was performed under the auspices of the U.S. Department of Energy by Univeristy of California, Lawrence Livermore National Laboratory under contract number W-7405-Eng-48.

7 REFERENCES

Al-Attar, L. and Dyer A. (2002) Sorption behaviour of uranium on birnessite, a layered manganese oxide. *Journal of Materials Chemistry* **12**, 1381-1386.

Appelo, C.A.J. and Postma D. (1999) A consistent model for surface complexation on birnessite (delta-MnO2) and its application to a column experiment. *Geochimica et Cosmochimica Acta* **63**, 3039-3048.

Axe, L., Tyson T., Trivedi P., and Morrison T. (2000) Local structure analysis of strontium sorption to hydrous manganese oxide. *Journal of Colloid and Interface Science* **224**, 408-416.

Balistrieri, L.S. and Murray J.W. (1982) The surface chemistry of delta-MnO2 in major ion seawater. *Geochimica et Cosmochimica Acta* **46**, 1041-1052.

Bethke C.M. (2002) *The Geochemist's Workbench: Release 4.0*. Software Package. University of Illinois, Urbana.

Carlos, B.A., Chipera S.J., Bish D.L., and Craven S.J. (1993) Fracture lining manganese oxide minerals in silicic tuff, Yucca Mountain, Nevada, USA. *Chemical Geology*, 107, 47-69.

Catts, J.G. and Langmuir D. (1986) Adsorption of Cu, Pb and Zn by delta-MnO2: applicability of the site binding-surface complexation model. *Applied Geochemistry* **1**, 255-264.

Chen, C.C., Golden D.C., and Dixon J.B. (1986) Transformation of synthetic birnessite to cryptomelane: an electron microscopic study. *Clays and Clay Minerals* **34** (5), 565-571.

Drellack, S.L, Jr., Prothro L.B., Roberson K.E., Schier B.A., and Price E.H. (1997) Analysis of Fractures in Volcanic Cores from Pahute Mesa, Nevada Test Site. Bechtel Nevada, DOE/NV/11718-160.

Duff, M.C., Hunter D.B., Triay I.R., Bertsch P.M., Reed D.T., Sutton S.R., Shea-McCarthy G., Kitten J., Eng P., Chipera S. J., and Vaniman D. T. (1999) Mineral associations and average oxidation states of sorbed Pu on tuff. *Environmental Science and Technology* **33**, 2163-2169.

Dyer, A., Pillinger M., Harjula R., and Amin S. (2000a) Sorption characteristics of radionuclides on synthetic birnessite-type layered manganese oxides. *Journal of Materials Chemistry* **10**(8), 1867-1874.

Dyer A., Pillinger M., Newton J., Harjula R., Moller T., and Amin S. (2000b) Sorption behavior of radionuclides on crystalline synthetic tunnel manganese oxides. *Chemistry of Materials* **12**(12), 3798-3804.

Dzombak D.A. and Morel F.M.M. (1990) Surface complexation modeling: hydrous ferric oxide. Wiley.

Foster, A.L., Brown G.E. Jr., and Parks G.A. (2003) X-ray absorption fine structure study of As (V) and SE (IV) sorption complexes on hydrous Mn oxides. *Geochimica et Cosmochimica Acta* **67** (11), 1937-1953.

Golden, D.C., Dixon J.B., and Chen C.C. (1986) on exchange, thermal transformations, and oxidizing properties of birnessite. *Clays and Clay Minerals* **34** (5), 511-520.

Herbelin, A.L. and Westall J.C. (1999) FITEQL: A computer program for determination of chemical equilibrium constants from experimental data. Department of Chemistry, Oregon State University, Corvallis.

Johnson J.W. and Lundeen S.R. (1997) GEMBOCHS thermodynamic datafiles for use with the EQ3/6 modeling package. Lawrence Livermore National Laboratory, Livermore, California.

Kennedy, C., Smith D.S., and Warren L.A. (2004) Surface chemistry and relative Ni sorptive capacities of synthetic hydrous Mn oxyhydroxides under variable wetting and drying regimes. *Geochimica et Cosmochimica Acta* **68** (3), 443-454.

Keeney-Kennicutt, W.L. and Morse J.W. (1984) The interaction of Np(V) O2+ with common mineral surfaces in dilute aqueous solutions and seawater. *Marine Chemistry* **15**, 133-150.

Keeney-Kennicutt, W.L. and Morse J.W. (1985) The redox chemistry of Pu(V)O2+ interaction with common mineral surfaces in dilute solutions and seawater. *Geochimica et Cosmochimica Acta* **49**, 2577-2588.

Kersting A.B. and Reimus P.W.E., Editors (2003) Colloid-Facilitated Transport of Low-solubility Radionuclides: A Field, Experimental, and Modeling Investigation. Lawrence Livermore National Laboratory, UCRL-ID-149688. Livermore, California.

Koeppenkastrop, D. and Carlo E.H.D. (1992) Sorption of rare-earth elements from seawater onto synthetic mineral particles: an experimental approach. *Chemical Geology* **95**, 251-263.

Loganathan, P. and Burau R.G. (1973) Sorption of heavy metal ions by a hydrous manganese oxide. *Geochimica et Cosmochimica Acta* **37**, 1277-1293.

Loganathan, P., Burau R.G., and Fuerstenau D.W. (1977) Influence of pH on the sorption of Co++, Zn++ and Ca++ by a hydrous manganese oxide. *Soil Science Society of America Journal* **41**, 57-62.

Manceau, A., Charlet L., Boisset M.C., Didier B., and Spadini L. (1992) Sorption and speciation of heavy metals on hydrous Fe and Mn oxides: from microscopic to macroscopic . *Applied Clay Science* **7**, 201-223.

Matocha, C.J., Elzinga E.J., and Sparks D.L. (2001) Reactivity of Pb(II) at the Mn(III,IV) (oxyhydr)oxide-water interface. *Environmental Science and Technology* **35** (14), 2967-2972.

McKenzie, R.M. (1979) Proton release during adsorption of heavy metal ions by a hydrous manganese dioxide. *Geochimica et Cosmochimica Acta* **43**, 1855-1857.

Means, J.L., Crerar D.A., Borcsik M.P., and Duguid J.O. (1978) Adsorption of Co and selected actinides by Mn and Fe oxides in soils and sediments. *Geochimica et Cosmochimica Acta* **42**, 1763-1773.

Misaelides, P., Katranas T., Godelitsas A., Lkewe-Nebenius H., and Anousis I. (2002) The chemical behavior of the natural microporous manganese-oxide todorokite in actinides (Th, U, Pa) aqueous solutions. *Separation Science and Technology* **37** (5), 1109-1121.

Murray, J.W. (1974) The surface chemistry of hydrous manganese dioxide. *Journal of Colloid and Interface Science* **46** (3), 357-371.

Murray, J.W. (1975) The interaction of metal ions at the manganese dioxide-solution interface. *Geochimica et Cosmochimica Acta* **39**, 509-519.

Olin, M. and Lehikoinen J. (1997) Application of surface complexation modeling: Nickel sorption on quartz, manganese oxide, kaolinite and goethite, and thorium on silica. Posiva Oy, Posiva 97-10. Helsinki, Finland.

O'Reilly, S.E. and Hochella M.F. Jr. (2003) Lead sorption efficiencies of natural and synthetic Mn and Fe-oxides. *Geochimica et Cosmochimica Acta* **67** (23), 4471-4487.

Parc, S., Nahon D., Tardy Y., and Vieillard P. (1989) Estimated solubility products and fields of stability for cryptomelane, nsutite, birnessite, and lithiophorite based on natural lateritic weathering sequences. *American Mineralogist* **74**, 466-475.

Posselt, H.S., Anderson F.J., and Weber W.J. Jr. (1968) Cation sorption on colloidal hydrous manganese dioxide. *Environmental Science and Technology* **2** (12), 1087-1093.

Post, J.E. (1999) Manganese oxide minerals: crystal structures and economic and environmental significance. *Proceedings of the National Academy of Science* **96**, 3446-3454.

Prothro, L.B. (1998) Analysis of Fractures in Cores from the Tuff Confining Unit Beneath Yucca Flat, Nevada Test Site. Bechtel Nevada, August, 1998.

Rose, T.P., Keneally J.M., Smith D.K., Davidson M.L., Hudson G.B. and Rego J.A.H. (1997) Chemical and isotope data for groundwater in Southern Nevada. Lawrence Livermore National Laboratory, UCRL-ID-128000. Livermore, California

Shaughnessy, D.A., Nitsche H., Booth C.H., Shuh D.K., Waychunas G.A., Wilson R.E., Gill H., Cantrell K.J., and Serne R.J. (2003) Molecular interfacial reactions between Pu(VI) and manganese oxide minerals manganite and hausmannite. *Environmental Science and Technology* **37** (15), 3367-3374.

Smith, R.W. and Jenne A.E. (1991) Recalculation, evaluation, and prediction of surface complexation constants for metal adsorption on iron and manganese oxides. *Environmental Science and Technology* **25** (3), 525-531.

Stahl, R.S. and James B.R. (1991) Zinc sorption by manganese-oxide-coated sand as a function of pH. *Soil Science Society of America Journal* **55**, 1291-1294.

Tamura, H., Katayama N., and Furuichi R. (1997) The Co^{2+} adsorption properties of Al2O3, Fe2O3, Fe3O4, TiO2, and MnO2 evaluated by modeling with the frumkin isotherm. *Journal of Colloid and Interface Science* **195**, 192-202.

Tanaka, Y. and Tsuji M. (1997) Thermodynamic study of alkaki metal ion exchanges on a manganese dioxide with hexagonal structure. *Materials Research Bulletin* **32** (4), 461-475.

Tessier, A., Fortin D., Belzile N., DeVitre R.R., and Leppard G.G. (1996) Metal sorption to diagenetic iron and manganese oxyhydroxides and associated organic matter: Narrowing the gap between field and laboratory measurements. *Geochimica et Cosmochimica Acta* **60**, 387-404.

Tonkin, J.W., Balistrieri L.S., and Murray J.W. (2004) Modeling sorption of divalent metal cations on hydrous manganese oxide using the diffuse double layer model. *Applied Geochemistry* **19**, 29-53.

Triay, I.R., Meijer A., Conca J.L., Kung K.S., Rundberg R.S., Strietelmeier B.A., Tait C.D., Clark D.L., Neu M.P., and Hobart D.E. (1997) Summary and synthesis report on radionuclide retardation of the Yucca Mountain Site Characterization Project. Yucca Mountain Site Characterization Program Milestone 3784M, pp. 274. Los Alamos National Laboratory.

Triay, I.R., Mitchell A.J., and Ott M.A. (1991) Radionuclide migration as a function of mineralogy. Los Alamos National Laboratory, LA-UR-91-113. Los Alamos, New Mexico.

Trivedi, P. and Axe L. (1999) A comparison of strontium sorption to hydrous aluminum, iron, and manganese oxides. *Journal of Colloid and Interface Science* **218**, 554-563.

Trivedi, P. and Axe L. (2001) Predicting divalent metal sorption to hydrous Al, Fe, and Mn oxides. *Environmental Science and Technology* **35** (9), 1779-1784.

Trivedi, P., Axe L., and Tyson T.A. (2001) XAS studies of Ni and Zn sorbed to hydrous manganese oxide. *Environmental Science and Technology* **35** (22), 4515-4521.

Turin, H.J., Groffman A.R., Wolfsberg L.E., Roach J.L., and Strietelmeier B.A. (2002) Tracer and radionuclide sorption to vitric tuffs of Busted Butte, Nevada. *Applied Geochemistry* **17**, 825-836.

Waychunas, G.A. (1991) Crystal chemistry of oxides and oxyhydroxides. *Reviews in Mineralogy* **25**, 11-68.

Zachara, J.M., Smith S.C., and Kuzel L.S. (1995) Adsorption and dissociation of Co-EDTA complexes in iron oxide-containing subsurface sands. *Geochimica et Cosmochimica Acta* **59** (23), 4825-4844.

Zavarin, M. (1999) Sorptive Properties of Synthetic and Soil Carbonates for Selenium, Nickel, and Manganese, Ph.D. Thesis, University of California at Berkeley.

Zavarin, M. and Bruton C.J. (2004a) A Non-Electrostatic Surface Complexation Approach to Modeling Radionuclide Migration at the Nevada Test Site:

Aluminosilicates. Lawrence Livermore National Laboratory, UCRL-TR-DRAFT. Livermore, California.

Zavarin, M. and Bruton C.J. (2004b) A Non-Electrostatic Surface Complexation Approach to Modeling Radionuclide Migration at the Nevada Test Site: Iron Oxides and Calcite. Lawrence Livermore National Laboratory, UCRL-TR-DRAFT. Livermore, California.

8 APPENDIX. BATCH SORPTION RAW DATA

Table A-1. Np-Sorption Data

Np-Manganese Oxides Sorption data

Volume in reaction tube 35 mL

Mass of mineral used: .05 g

Initial Np conc., M 3.5E-06

Sampling time: 3 day		Sampling time: 17 days		Sampling time: 27 days		
pH	% Sorption	pH	% Sorption	pH	% Sorption	Kd,mL/g
2.84	0.00%	2.83	3.33%	2.8	8.01%	60.7
3.78	0.00%	3.74	0.0%	3.60	7.5%	56.0
3.8	0.01%	3.78	2.45%	3.74	6.21%	46.0
5.45	0.57%	5.54	4.75%	5.43	10.18%	78.7
6.19	6.11%	6.28	7.6%	6.42	17.6%	148.7
6.56	9.71%	7.01	24.47%	7.15	32.94%	343.8
7.44	30.21%	7.72	45.53%	7.80	57.5%	943.6
7.52	36.76%	7.74	52.3%	7.96	61.6%	1123.6
7.68	41.39%	7.86	56.2%	7.99	55.60%	873.2
7.96	48.26%	8.18	58.8%	8.28	62.9%	1183.1
8.51	49.04%	8.58	52.0%	8.58	56.1%	891.7
9.07	48.34%	9.00	53.4%	8.95	54.9%	846.5
10.00	50.15%	9.84	55.4%	9.75	57.5%	947.7

Np-Cryptomelane sorption

Sampling time: 3 day		Sampling time: 17 days		Sampling time: 27 days		
pH	% Sorption	pH	% Sorption	pH	% Sorption	Kd, mL/g
3.30	1.83%	3.27	2.4%	3.20	7.6%	57.1
4.29	0.00%	4.36	0.9%	4.30	6.1%	45.9
5.40	1.26%	5.43	2.3%	5.32	7.5%	56.8
5.90	1.20%	5.95	5.2%	5.88	8.9%	68.0
7.24	12.01%	7.25	19.3%	7.44	29.5%	291.2
8.16	36.53%	8.31	47.3%	8.45	54.0%	821.4
9.15	43.10%	9.05	45.5%	8.88	50.0%	698.8
10.03	40.32%	9.92	47.7%	9.79	49.5%	682.1

Np-Pyrolusite sorption

Sampling time: 3 day		Sampling time: 17 days		Sampling time: 27 days		
pH	% Sorption	pH	% Sorption	pH	% Sorption	Kd, mL/g
3.28	0.00%	3.25	0.0%	3.10	5.9%	44.2
3.94	0.00%	4.00	0.0%	3.97	5.3%	38.7
5.60	0.45%	5.97	2.8%	6.06	11.2%	88.5
6.62	5.17%	6.97	12.3%	7.14	19.8%	173.4
7.65	20.93%	8.02	37.7%	8.12	43.7%	534.5
8.26	25.76%	8.43	35.5%	8.50	40.0%	461.8
9.03	33.73%	8.90	35.3%	8.81	39.0%	446.6
9.95	38.55%	9.89	38.2%	9.77	40.4%	471.3

Table A-2. Np-Desorption data.

Np-Manganese Oxides Desorption data
Volume in reaction tube 35 mL
Mass of mineral uesd: .05 g

Np-Birnessite Desorption

Sampling time: 1 days				Sampling time: 15 days			Sampling time: 33 days			
pH	initial Np, mmoles	desorbed mmoles	% Sorption	pH	desorbed mmoles	% Sorption	pH	desorbed mmoles	% Sorption	Kd,mL/g
3.02	9.81E-06	1.72E-06	82.4%	3.07	1.75E-06	82.2%	3.08	1.95E-06	80.1%	2813.298
3.17	9.14E-06	2.18E-06	76.1%	3.17	2.51E-06	72.6%	3.18	2.28E-06	75.1%	2105.861
3.55	7.61E-06	2.02E-06	73.4%	3.57	2.05E-06	73.0%	3.62	2.14E-06	71.9%	1791.918
5.14	2.16E-05	1.44E-05	33.1%	5.35	1.47E-05	32.1%	3.80	4.98E-06	60.1%	1054.689
5.62	1.25E-05	5.15E-06	58.7%	5.74	4.87E-06	60.9%	5.34	1.53E-05	29.1%	287.6652
6.38	7.04E-05	5.65E-05	19.7%	6.89	2.57E-05	36.4%	7.00	2.57E-05	36.4%	400.5586
6.65	4.04E-05	2.80E-05	30.7%	7.35	4.01E-05	43.0%	7.72	3.05E-05	56.7%	917.0676
6.75	7.55E-05	5.54E-05	26.6%	7.65	3.64E-05	51.8%	7.93	2.91E-05	61.4%	1115.304
7.32	7.70E-05	4.33E-05	43.8%	7.77	3.14E-05	53.9%	7.95	3.02E-05	55.6%	877.9574
7.48	6.81E-05	3.70E-05	45.6%	8.11	3.29E-05	57.3%	8.38	2.97E-05	61.4%	1114.065
8.20	6.87E-05	2.65E-05	61.4%	8.56	2.77E-05	59.7%	8.68	2.67E-05	61.1%	1099.547
9.02	6.72E-05	2.37E-05	64.7%	9.07	2.59E-05	61.5%	9.02	2.53E-05	62.4%	1160.067
9.98	7.05E-05	2.19E-05	68.9%	9.96	2.31E-05	67.2%	9.96	2.35E-05	66.6%	1397.223

Np-Cryptomelane Desorption

Sampling time: 1 days				Sampling time: 15 days			Sampling time: 33 days			
pH	initial Np, mmoles	desorbed mmoles	% Sorption	pH	desorbed mmoles	% Sorption	pH	desorbed mmoles	% Sorption	Kd,mL/g
3.05	9.25E-06	2.00E-06	78.4%	3.08	2.10E-06	77.3%	3.11	1.90E-06	79.5%	2713.097
3.87	7.53E-06	2.71E-06	64.0%	3.95	2.94E-06	61.0%	4.03	2.71E-06	64.1%	1247.318
5.59	9.25E-06	3.84E-06	58.5%	6.00	4.04E-06	56.3%	6.16	3.70E-06	60.0%	1051.095
6.39	1.09E-05	4.99E-06	54.4%	7.20	3.69E-06	66.3%	7.68	2.01E-06	81.6%	3112.746
7.21	3.62E-05	2.62E-05	27.5%	7.52	2.01E-05	44.4%	7.74	1.63E-05	54.9%	852.0243
8.17	6.62E-05	3.64E-05	45.1%	8.51	3.10E-05	53.2%	8.60	2.91E-05	56.1%	894.2491
9.14	6.12E-05	3.13E-05	48.8%	9.05	3.01E-05	50.9%	9.03	2.99E-05	51.1%	730.9958
10.07	6.06E-05	2.92E-05	51.9%	10.00	3.04E-05	49.7%	9.99	3.05E-05	49.6%	689.3101

Np-Pyrolusite Desorption

Sampling time: 1 days				Sampling time: 15 days			Sampling time: 33 days			
pH	initial Np, mmoles	desorbed mmoles	% Sorption	pH	desorbed mmoles	% Sorption	pH	desorbed mmoles	% Sorption	Kd,mL/g
3.00	7.25E-06	7.33E-07	89.9%	3.04	6.36E-07	91.2%	2.97	6.77E-07	90.7%	6797.248
3.40	6.51E-06	1.64E-06	74.9%	3.43	1.70E-06	73.9%	3.37	1.49E-06	77.2%	2364.539
5.06	1.37E-05	6.48E-06	52.7%	6.11	6.30E-06	54.0%	6.74	5.96E-06	56.5%	907.805
6.29	2.42E-05	1.50E-05	37.9%	7.26	1.32E-05	45.6%	7.72	9.65E-06	60.1%	1055.298
7.19	5.35E-05	3.14E-05	41.4%	8.00	2.69E-05	49.7%	8.34	2.38E-05	55.5%	872.0654
8.01	4.90E-05	2.24E-05	54.4%	8.43	2.43E-05	50.3%	8.57	2.32E-05	52.7%	778.935
9.04	4.78E-05	2.15E-05	55.1%	9.00	2.37E-05	50.4%	8.93	2.42E-05	49.3%	681.5088
10.01	4.95E-05	2.18E-05	56.0%	9.98	2.47E-05	50.1%	9.92	2.60E-05	47.6%	634.8965

Table A-3. Np batch-sorption major cation analyses (mol/ L).

Birnessite

pH	HCO_3^-	Na^+	K^+	Mg^{2+}	Mn^{2+}	Ca^{2+}
3.18	7.86E-05	1.71E-02	2.30E-04	1.46E-05	1.27E-03	6.54E-05
5.34	8.26E-05	1.69E-02	1.60E-04	1.23E-06	8.20E-05	4.22E-06
7.72	8.06E-05	1.40E-02	2.98E-04	(nd)*	1.42E-05	(nd)
7.93	1.68E-04	1.19E-02	1.44E-04	(nd)	7.67E-06	(nd)
8.38	9.37E-04	1.04E-02	1.36E-04	(nd)	4.82E-06	(nd)
8.68	1.80E-03	1.11E-02	1.81E-04	(nd)	1.08E-05	(nd)
9.02	2.02E-03	1.08E-02	1.92E-04	(nd)	9.56E-06	(nd)
9.96	2.30E-03	1.08E-02	3.44E-04	(nd)	8.81E-06	(nd)

Cryptomelane

pH	HCO_3^-	Na^+	K^+	Mg^{2+}	Mn^{2+}	Ca^{2+}
3.11	7.77E-05	8.72E-03	1.95E-03	1.22E-05	1.24E-03	6.28E-05
4.03	8.24E-05	1.09E-02	2.12E-03	1.14E-06	1.03E-03	2.29E-05
6.16	9.19E-05	8.88E-03	1.44E-03	6.67E-07	6.66E-04	1.31E-05
7.68	1.63E-04	7.94E-03	1.14E-03	2.30E-07	3.94E-04	7.14E-06
7.74	1.56E-04	7.46E-03	9.51E-04	(nd)	2.48E-05	(nd)
8.60	1.05E-03	1.09E-02	1.38E-03	(nd)	1.10E-05	(nd)
9.03	1.38E-03	9.67E-03	1.03E-03	(nd)	5.86E-06	(nd)
9.99	1.66E-03	1.21E-02	8.35E-04	(nd)	2.51E-06	(nd)

Pyrolusite

pH	HCO_3^-	Na^+	K^+	Mg^{2+}	Mn^{2+}	Ca^{2+}
2.97	7.78E-05	9.33E-03	4.54E-04	1.04E-05	1.79E-04	4.34E-05
3.37	7.72E-05	1.01E-02	5.27E-04	2.14E-06	1.77E-04	4.47E-06
6.74	8.26E-05	9.56E-03	5.33E-04	1.06E-06	6.69E-05	2.35E-06
7.72	7.31E-05	9.11E-03	7.80E-04	(nd)	1.17E-05	(nd)
8.34	8.53E-04	9.32E-03	8.57E-04	(nd)	3.55E-06	(nd)
8.57	1.11E-03	6.21E-03	3.91E-04	(nd)	1.16E-06	(nd)
8.93	2.09E-03	7.55E-03	6.14E-04	(nd)	1.16E-06	(nd)
9.92	1.92E-03	1.18E-02	8.37E-04	(nd)	8.29E-07	(nd)

* (nd) indicates that the species of interest was not detected at that pH.

Table A-4. Pu-Sorption Data.

Pu-Manganese Oxides Sorption data

Volume in reaction tube: 35 mL

Mass of mineral used: 0.01g

Initial Pu conc., M 4.94E-09

Pu-Birnessite sorption

Sampling time: 1 day		Sampling time: 19 days		Sampling time: 34 days		
pH	% Sorption	pH	% Sorption	pH	% Sorption	Kd, mL/g
3.22	3.4%	3.26	7.4%	3.20	9.3%	3.48E+02
4.71	47.0%	4.76	86.1%	4.74	89.6%	3.02E+04
5.77	78.5%	6.06	97.8%	6.35	98.6%	2.38E+05
6.81	96.8%	7.25	98.9%	7.56	99.9%	2.50E+06
7.75	96.7%	8.06	98.9%	8.27	99.4%	5.86E+05
8.54	95.2%	8.56	97.9%	8.59	97.9%	1.57E+05
9.11	90.1%	9.10	93.2%	8.97	93.2%	4.66E+04
9.95	91.3%	9.95	96.6%	9.90	97.0%	1.12E+05

Pu-Cryptomelane sorption

Sampling time: 1 day		Sampling time: 19 days		Sampling time: 34 days		
pH	% Sorption	pH	% Sorption	pH	% Sorption	Kd, mL/g
3.22	0.35%	3.30	0.04%	3.23	0.27%	9.53E+00
4.08	16.54%	4.22	33.48%	4.13	34.46%	1.75E+03
5.19	67.15%	5.45	90.32%	5.60	92.82%	4.44E+04
6.71	99.61%	7.11	100.00%	7.43	99.99%	2.41E+07
7.78	99.44%	8.06	99.47%	8.31	99.38%	5.55E+05
8.32	92.75%	8.53	98.16%	8.52	98.43%	2.17E+05
9.15	91.62%	9.15	95.75%	9.09	96.68%	1.02E+05
9.97	94.91%	10.00	95.66%	9.90	96.02%	8.11E+04

Pu-Pyrolusite sorption

Sampling time: 1 day		Sampling time: 19 days		Sampling time: 34 days		
pH	% Sorption	pH	% Sorption	pH	% Sorption	Kd, mL/g
3.27	14.97%	3.28	19.44%	3.18	19.48%	8.38E+02
4.30	71.42%	4.40	95.37%	4.36	97.12%	1.16E+05
5.56	97.35%	5.98	99.90%	6.36	99.72%	1.21E+06
6.84	99.68%	7.22	99.61%	7.59	99.97%	1.11E+07
7.73	98.45%	8.02	99.63%	8.25	99.58%	8.07E+05
8.34	67.38%	8.48	70.00%	8.53	71.84%	8.67E+03
9.04	79.84%	9.02	83.35%	8.90	84.36%	1.83E+04
9.97	94.50%	9.97	95.42%	9.88	95.47%	7.09E+04

Table A-5. Pu-Desorption Data.

Pu-Manganese Oxides Desorption data
Volume in reaction tube 35 mL
Mass of mineral uesd: 0.01g

Pu-Birnessite Desorption

Sampling time: 2 days				Sampling time: 16 days			Sampling time: 22 days			
pH	initial Pu, mmoles	desorbed mmoles	% Sorption	pH	desorbed mmoles	% Sorption	pH	desorbed mmoles	% Sorption	Kd, mL/g
3.22	1.61E-08	1.00E-08	37.5%	3.32	1.26E-08	21.9%	3.23	1.30E-08	19.2%	8.33E+02
4.26	1.55E-07	2.53E-08	83.7%	4.34	2.4581E-08	84.1%	4.26	2.27E-08	85.4%	2.04E+04
6.00	1.70E-07	4.96E-09	97.1%	6.20	3.25991E-09	98.1%	6.26	2.51E-09	98.5%	2.35E+05
6.85	1.73E-07	1.40E-09	99.2%	7.07	1.4563E-09	99.2%	7.22	1.15E-09	99.3%	5.21E+05
7.85	1.72E-07	6.44E-10	99.6%	8.00	1.18306E-09	99.3%	8.08	1.16E-09	99.3%	5.15E+05
8.44	1.69E-07	4.68E-10	99.7%	8.52	9.5185E-10	99.4%	8.51	1.01E-09	99.4%	5.80E+05
9.05	1.61E-07	4.18E-10	99.7%	9.00	1.05895E-09	99.3%	9.02	1.24E-09	99.2%	4.50E+05
9.98	1.68E-07	5.42E-10	99.7%	9.95	9.33834E-10	99.4%	9.95	9.46E-10	99.4%	6.17E+05

Pu-Cryptomelane Desorption

Sampling time: 2 days				Sampling time: 16 days			Sampling time: 22 days			
pH	initial Pu, mmoles	desorbed mmoles	% Sorption	pH	desorbed mmoles	% Sorption	pH	desorbed mmoles	% Sorption	Kd, mL/g
3.23	4.74E-10	2.85E-10	39.8%	3.26	5.08E-10	0.0%	3.21	4.98E-10	0.0%	0.00E+00
4.10	5.96E-08	3.14E-08	47.3%	4.09	3.21E-08	46.2%	4.06	3.29E-08	44.7%	2.83E+03
5.93	1.60E-07	5.11E-09	96.8%	5.93	4.37E-09	97.3%	6.00	3.92E-09	97.6%	1.40E+05
6.71	1.73E-07	3.14E-10	99.8%	6.97	2.13E-10	99.9%	7.05	1.59E-10	99.9%	3.81E+06
7.83	1.72E-07	1.01E-09	99.4%	8.01	9.18E-10	99.5%	8.09	1.74E-09	99.0%	3.43E+05
8.40	1.70E-07	9.59E-10	99.4%	8.51	9.40E-10	99.4%	8.51	1.13E-09	99.3%	5.24E+05
9.03	1.67E-07	8.34E-10	99.5%	8.98	9.53E-10	99.4%	8.90	1.11E-09	99.3%	5.24E+05
10.30	1.66E-07	1.29E-09	99.2%	10.01	1.80E-09	98.9%	9.92	1.59E-09	99.0%	3.62E+05

Pu-Pyrolusite Desorption

Sampling time: 2 days				Sampling time: 16 days			Sampling time: 22 days			
pH	initial Pu, mmoles	desorbed mmoles	% Sorption	pH	desorbed mmoles	% Sorption	pH	desorbed mmoles	% Sorption	Kd, mL/g
3.24	3.37E-08	8.53E-09	74.7%	3.23	1.42E-08	58.0%	3.21	1.53E-08	54.6%	4.21E+03
4.05	1.68E-07	1.62E-08	90.4%	4.05	1.20E-08	92.8%	3.99	9.80E-09	94.2%	5.65E+04
5.59	1.72E-07	6.07E-10	99.6%	5.86	1.72E-10	99.9%	6.01	1.55E-10	99.9%	3.89E+06
6.67	1.73E-07	2.12E-10	99.9%	6.92	4.80E-11	100.0%	7.03	6.39E-11	100.0%	9.46E+06
7.76	1.72E-07	4.49E-10	99.7%	7.93	3.46E-10	99.8%	8.05	3.43E-10	99.8%	1.76E+06
8.39	1.24E-07	3.69E-09	97.0%	8.53	3.15E-09	97.5%	8.56	4.88E-09	96.1%	8.57E+04
9.00	1.46E-07	2.97E-09	98.0%	8.96	2.24E-09	98.5%	8.92	2.87E-09	98.0%	1.74E+05
10.03	1.65E-07	3.05E-09	98.2%	9.99	2.12E-09	98.7%	9.95	2.69E-09	98.4%	2.11E+05

Table A-6. Pu batch-sorption major cation analyses (mol/ L).

Birnessite

pH	HCO_3^-	Na^+	K^+	Mg^{2+}	Mn^{2+}	Ca^{2+}
3.20	7.35E-05	1.10E-02	7.04E-04	1.04E-05	5.07E-04	3.27E-05
4.74	7.14E-05	1.07E-02	4.88E-04	2.67E-06	3.37E-04	5.18E-06
6.35	8.63E-05	1.08E-02	4.35E-04	1.46E-06	1.45E-04	1.25E-06
7.56	1.21E-03	1.10E-02	3.54E-04	8.72E-07	2.13E-05	4.99E-06
8.27	3.28E-03	9.84E-03	9.71E-04	9.22E-07	1.12E-05	4.99E-06
8.59	4.21E-03	9.70E-03	4.69E-04	8.80E-07	8.60E-06	4.99E-06
8.97	4.48E-03	1.02E-02	2.48E-04	1.07E-06	1.09E-05	4.99E-06
9.90	4.78E-03	1.23E-02	2.46E-04	1.03E-06	4.16E-06	4.99E-06

Cryptomelane

pH	HCO_3^-	Na^+	K^+	Mg^{2+}	Mn^{2+}	Ca^{2+}
3.23	7.49E-05	9.87E-03	2.22E-03	8.39E-06	4.29E-04	2.55E-05
4.13	7.18E-05	9.71E-03	1.26E-03	4.11E-06	4.21E-04	9.81E-06
5.60	7.36E-05	9.21E-03	1.14E-03	1.88E-06	2.70E-04	2.74E-06
7.43	1.02E-03	9.86E-03	9.41E-04	1.04E-06	3.47E-05	(nd)
8.31	3.82E-03	9.50E-03	9.49E-04	9.30E-07	1.21E-05	(nd)
8.52	4.63E-03	9.46E-03	8.38E-04	1.04E-06	9.02E-06	(nd)
9.09	5.00E-03	9.39E-03	9.42E-04	1.05E-06	7.37E-06	(nd)
9.90	5.11E-03	1.19E-02	9.08E-04	1.07E-06	8.71E-06	(nd)

Pyrolusite

pH	HCO_3^-	Na^+	K^+	Mg^{2+}	Mn^{2+}	Ca^{2+}
3.18	1.24E-04	9.52E-03	4.26E-04	1.11E-05	7.14E-05	3.33E-05
4.36	1.29E-04	1.00E-02	5.99E-04	3.94E-06	5.87E-05	9.88E-06
6.36	7.86E-05	9.26E-03	6.22E-04	1.96E-06	2.00E-05	(nd)
7.59	1.02E-03	9.68E-03	1.35E-03	1.71E-06	6.17E-06	(nd)
8.25	2.80E-03	9.98E-03	1.30E-03	1.41E-06	2.35E-06	(nd)
8.53	4.10E-03	9.80E-03	8.88E-04	1.30E-06	3.70E-06	(nd)
8.90	4.31E-03	9.83E-03	5.12E-04	1.22E-06	2.01E-06	(nd)
9.88	4.26E-03	1.20E-02	7.20E-04	1.15E-06	6.94E-07	(nd)